A Novel Diffusion-based Empirical Mode Decomposition Algorithm for Signal and Image Analysis

by

Heming Wang

A thesis
presented to the University of Waterloo
in fulfillment of the
thesis requirement for the degree of
Master of Mathematics
in
Applied Mathematics

Waterloo, Ontario, Canada, 2018

I hereby declare that I am the sole author of this thesis. This is a true copy of the thesis, including any required final revisions, as accepted by my examiners.

I understand that my thesis may be made electronically available to the public.

Abstract

In the area of signal analysis and processing, the Fourier transform and wavelet transform are widely applied. Empirical Mode Decomposition(EMD) was proposed as an alternative frequency analysis tool. Although shown to be effective when analyzing non-stationary signals, the algorithmic nature of EMD makes the theoretical analysis and formulation difficult. Futhermore, it has some limitations that affect its performance.

In this thesis, we introduce some methods to extend or modify EMD, in an effort to provide a rigorous mathematical basis for it, and to overcome its shortcomings. We propose a novel diffusion-based EMD algorithm that replaces the interpolation process by a diffusion equation, and directly construct the mean curve (surface) of a signal (image). We show that the new method simplifies the mathematical analysis, and provides a solid theory that interprets the EMD mechanism. In addition, we apply the new method to the 1D and 2D signal analysis showing its possible applications in audio and image signal processing. Finally, numerical experiments for synthetic and real signals (both 1D and 2D) are presented. Simulation results demonstrate that our new algorithm can overcome some of the shortcomings of EMD, and require much less computation time.

Acknowledgements

First of all, I would like to thank my supervisors, Prof. R. Mann and Prof. E. R. Vrscay for their dedication, support and patience during my master study. This thesis would not have been completed without them. I would also like to thank Prof. G. Freeman, Department of Electrical and Computer Engineering, UW and Prof. G. Tran, Department of Applied Mathematics, UW for their willingness to act as readers and examiners of this thesis. Their questions, comments and suggestions certainly helped to improve the quality of thesis and were very much appreciated.

Also I would like to thank my fellow graduate students and friends for all the encouragement and useful discussions during my thesis writing.

Finally, I am thankful to my family for their unconditional love and support.

Table of Contents

List of Tables

List of Figures

Chapter 1

Introduction

1.1 Introduction

Time-frequency analysis is a powerful tool to analyze signals. For a complex time series, time-frequency representation can reveal its structure and give insight to different components within the signal, e.g., the phonemes in speech utterance, vibrations in motors and seismic waves in earthquakes. In addition, time-frequency analysis can be extended to two or even higher dimensions, and applied in image and video processing.

Among all the various time-frequency analysis methods, the two most popular ones are Fourier transform and wavelet transform. Fourier transform regards all signals as a mixture of different sinusoids. Each sinusoid is a single frequency component within the signal. One shortcoming of Fourier transform is that it neglects the time information, and therefore cannot represent some transient features within the signal. To solve this problem, short-time Fourier Transform (STFT) was introduced [1]. The idea of STFT is to perform the Fourier transform over shorter components of the signal in order to obtain local frequency sprectra. However, the method is still limited due to the restriction of "uncertainty principle", which means we can have either temporal or spectral locality regarding the information contained in the signal, but never both. Instead of treating the signal as a mixture of sinusoids, the wavelet transform uses a self-defined function called the *mother wavelet* to represent the signal. The wavelet function can be translated and scaled to fit the signal that is being analyzed. This way, the wavelet transform can find the localized information contained in the signal with desired resolutions.

Empirical Mode Decomposition (EMD) is another method developed for time-frequency analysis. Proposed by Huang et al. [18] in 1998, it aims to decompose a signal as a mixture

of components that are well-separated in the time-frequency plane. Each of the components can be viewed as a harmonic that has a slowly-varying magnitude. When combined with the Hilbert transform, it can output the time-varying local frequency component at each time using phase information. EMD has been applied quite successfully in science and engineering, for instance, engine vibration [19], earthquake analysis [18] and medical imaging [2]. Although EMD has proved its powerfulness in signal analysis, its empirical nature has made it difficult to analyze theoretically. The lack of theoretical background limits the application of EMD. For instance, EMD fails to separate different frequency components when there exist "intermittency" in the signal [32], and EMD also has limited separation capability. All these problems require a theoretical explanation, so that we can have a quantitative analysis and further improve the method.

EMD procedures rely on the location of local maxima and minima of a signal followed by interpolation to find upper and lower envelope curves, which are then used to extract a "mean curve" of a signal. These operations are not only sensitive to noise and error, but they also present difficulties for a mathematical analysis of EMD. To solve this problem, we propose a novel PDE-based algorithm as an alternative to EMD algorithm. Our PDE-based approach replaces the above procedures by simply using the diffusion equation to construct the mean curve (surface) of a signal (image). This procedure also simplifies the mathematical analysis.

In this chapter, we will briefly introduce several methods in time-frequency analysis. These methods, including Fourier transform, wavelet transform and Hilbert transform, are widely applied in practice. Depending on the application scenario, each method has its own advantages and its limitations.

The rest of the thesis is organized as follows: Chapter 2 introduces the details of the classical EMD algorithm. In Chapter 3 are discussed related works that try to build a theoretical framework for EMD. Chapter 4 introduces our novel method, which applies the diffusion equation to extract Intrinsic Mode Functions from signal. In Chapter 5 we present some extensions of the classical EMD method. In Chapter 6 we provide a 2D extension for the new diffusion-based method. Chapter 7 is the conclusion of the thesis, where the limitations and potential work of our proposed method are also included.

1.2 Fourier Analysis

The most widely applied method in signal processing has been Fourier analysis. Fourier analysis decomposes a signal into sinusoids of different frequency components. A periodic

signal can be expressed in terms of a Fourier series. A non-periodic signal over the entire real line can be analyzed with Fourier transform.

1.2.1 Fourier Series

A signal $f(t)$ of period T can be expressed as the following Fourier series.

$$f(t) = \frac{a_0}{2} + \sum_{k=1}^{\infty} a_k cos(k\omega_0 t) + \sum_{k=1}^{\infty} b_k sin(k\omega_0 t),\ -\frac{T}{2} \leq t \leq \frac{T}{2}\,. \tag{1.1}$$

Here $\omega_0 = \frac{2\pi}{T}$ is the fundamental angular frequency. The Fourier coefficients for the series can be obtained as follows:

$$a_0 = \frac{2}{T}\int_{-T/2}^{T/2} f(t)dt \tag{1.2}$$

$$a_k = \frac{2}{T}\int_{-T/2}^{T/2} f(t)\cos(k\omega_0 t)dt\,, k = 1, 2, 3, ... \tag{1.3}$$

$$b_k = \frac{2}{T}\int_{-T/2}^{T/2} f(t)\sin(k\omega_0 t)dt\,, k = 1, 2, 3, ...\,. \tag{1.4}$$

In a Hilbert space X, let $e_1, e_2, ..., e_n$ be an orthonormal set. Let S_n be the span of these linearly independent elements e_i, $1 \leq i \leq n$,

$$S_n = \{x \in X \,|\, x = c_1 e_1 + c_2 e_2 + ... + c_n e_n\}\,. \tag{1.5}$$

For an arbitrary element $x \in X$, we aim to find the best approximation v to x in the subspace S_n, i.e, the closest element within S_n to x measured by the norm on X.

$$y_n = \arg\min_{v \in S_n} ||x - v||\,. \tag{1.6}$$

It is well known that the best approximation of x in S_n is given by the unique element

$$\begin{aligned} v &= c_1 e_1 + c_2 e_2 + ... + c_n e_n \\ &= \sum_{k=1}^{n} c_k e_k\,, \end{aligned} \tag{1.7}$$

where $\{c_k\}_{k=1}^n$ is the unique set of "Fourier coefficients" given by

$$c_k = \langle x, e_k \rangle, \quad k = 1, 2, ..., n\,. \tag{1.8}$$

Furthermore, if we have an infinite sequence of orthonormal elements $\{e_n\}_{n=1}^{\infty}$, and this sequence forms a complete basis in H, the best approximation errors will go to zero in the limit. This means we can represent any element in H with an complete orthonormal set. The essence of Fourier series is to represent the signal by the orthonormal basis $\{\frac{2}{T}\sin(m\omega t), \frac{2}{T}\cos(n\omega t)\}$. According to the analysis above, the Fourier representation of any signal is unique.

1.2.2 Fourier Transform

For an integrable function f defined on the real line $\mathbb{R}$, the Fourier transform can be defined as

$$F(\omega) = \frac{1}{\sqrt{2\pi}} \int_{-\infty}^{\infty} f(t) e^{-i\omega t} dt \,. \tag{1.9}$$

Its inverse is given by:

$$f(t) = \frac{1}{\sqrt{2\pi}} \int_{-\infty}^{\infty} F(\omega) e^{i\omega t} d\omega \,. \tag{1.10}$$

The discrete Fourier transform (DFT) extends the application to discrete sampled signal. By employing the following orthonormal basis

$$e_k[n] = \frac{1}{\sqrt{N}} \exp(\frac{i2\pi kn}{N}) \,, \quad n = 0, 1, ..., N-1 \,, z \tag{1.11}$$

The DFT of a function f is defined as

$$F[k] = \frac{1}{\sqrt{N}} \sum_{n=0}^{N-1} f[n] \exp(-\frac{i2\pi kn}{N}) \,, \quad k = 0, 1, ..., N-1 \,. \tag{1.12}$$

and the inverse DFT is

$$f[n] = \frac{1}{\sqrt{N}} \sum_{k=0}^{N-1} F[k] \exp(\frac{i2\pi kn}{N}) \,, \quad n = 0, 1, ..., N-1 \,. \tag{1.13}$$

Fourier transform is widely applied and has become the standard technique to obtain frequency information about a signal. Despite the success of Fourier transform, it cannot provide any temporal information of the signal. To retain the time information of a signal, we introduce the short time Fourier transform, in order to deal with non-stationary signals.

1.2.3 Short-time Fourier Transform

In STFT, we apply the FFT to finite length possibly overlapping segments of input. Each segment has a weighted window function applied. A window function is a continuous function, close to unity at the center and approximate zero-value towards the edges. By applying an appropriate window function, we can obtain a good localization in both time and frequency domains. Typical window used includes trianular, raised cosine, Hanning, etc.

When applying STFT, the signal is multiplied by the window function at a certain segment. After Fourier transform is done on that segment, the window will be moved to the next slice and repeat the same operation. STFT can be expressed as follows:

$$STFTf(\omega, b) = \frac{1}{\sqrt{2\pi}} \int_{-\infty}^{\infty} f(t)g(t-b)e^{-i\omega t}dt\,. \tag{1.14}$$

where $g(t)$ is the window function, and $g(t-b)$ is the window that applied at location b. A window function $g(t)$ should be normalized and has zero value outside a certain interval C, i.e.

$$\begin{aligned} &\int_{-\infty}^{\infty} g(t)dt = 1 \\ &g(t) = 0, \quad for\,|t| \geq C\,, \end{aligned} \tag{1.15}$$

The inverse STFT can reconstruct the signal by doing:

$$f(t) = \frac{1}{\sqrt{2\pi}} \int_{-\infty}^{\infty} \int_{-\infty}^{\infty} STFTf(\omega, b)g(t-b)e^{i\omega t}dtd\omega. \tag{1.16}$$

The shortcoming of the STFT method is that the resolution for the time-frequency spectrum has fixed resolution in both time and frequency axes. In frequency spectrum, sometimes high frequency region contains more information compared with low frequency region, as high frequency components tend to vary faster. Therefore we require higher resolution for the high frequency components and lower resolution for low frequency components. The wavelet transform has been developed to tackle this problem.

1.3 Wavelet Transform

Developed by Grossman and Morlet [16], wavelet analysis is a powerful tool which provides different resolutions for different frequency regions. The purpose of wavelet transform is

to provide a tool to analyze the non-stationary signal. In wavelet transform, signal will be decomposed into a series of wavelet basis. A wavelet basis function generally has compact support, so that it is localized in time and frequency to serve as the basis function. The essence is wavelet transform is that we form a set of orthonormal basis functions by suitable scaling and translating the wavelet basis. Therefore using wavelet basis we can represent frequency spectrum with different resolution.

1.3.1 Continuous Wavelet Transform

Continuous Wavelet transform (CWT) can operate at different scales and positions. Like the name, the CWT is continuous and can be shifted smoothly over the domain of the analyzed signal.

The mother wavelet is denoted as $\psi(t)$, and all other wavelets can be expanded by scaling and translating as follows:

$$\psi_{a,b} = \frac{1}{\sqrt{a}}\psi(\frac{t-b}{a}). \tag{1.17}$$

The continuous wavelet transform has the following form:

$$W_\psi f_{a,b} = \frac{1}{\sqrt{a}}\int_{-\infty}^{\infty} f(t)\overline{\psi(\frac{t-b}{a})}dt, \tag{1.18}$$

where $a, b \in \mathbb{R}, a \neq 0$ is the parameter that controls the scaling, b defines the translation, and $\frac{1}{\sqrt{a}}$ is the normalization factor. After scaling parameter and translating parameter are chosen, a group of wavelets will be generated according to the a's and b's. In this way the function $f(t)$ is multiplied by the mother wavelet at different locations and scales. The inverse wavelet transform is given by:

$$f(t) = \frac{1}{2\pi C_\psi}\int_{-\infty}^{\infty}\int_{-\infty}^{\infty}\frac{W_\psi f_{a,b}}{a^2}\psi_{a,b}(t)\,da\,db\,, \tag{1.19}$$

where

$$C_\psi = \int_{-\infty}^{\infty}\frac{|\hat{\psi}(w)|^2}{|\omega|}d\omega\,, \tag{1.20}$$

and $\hat{\psi}(\omega)$ is the Fourier transform of $\psi(t)$. Most commonly used wavelets include Haar, Daubechies [7], Morlet, Mexican Hat. Properly chosen wavelets can decompose signals into well-behaved signal spaces.

1.3.2 Discrete Wavelet Transform (DWT)

In contrast to CWT, the discrete wavelet transform (DWT) of a discrete signal employs discrete frequencies and is more efficient. The major difference between CWT and DWT is that DWT uses frequency only in the octave. Specifically a and b will be replaced by $a_j = \frac{1}{2^j}$ and $b = ka_j$ for some $j, k \in \mathbb{Z}$,

$$DWT_\psi f[n] = \frac{1}{\sqrt{a_j}} \sum_k f[k]\psi(\frac{n - ka_j}{a_j}) \,. \tag{1.21}$$

In practice, DWT implementation will introduce pairs of high-pass and low-pass filters at each scaling stage of the transform. DWT is computationally less expensive, and has been widely applied in signal compression.

Wavelet makes it possible to have a good resolution in both time and frequency domain, However, the performance highly depends on the mother wavelet that we choose. It is hard to select the most appropriate wavelet for the specific signal, and sometimes it requires prior knowledge of the frequency component to find the best wavelet.

1.4 Hilbert Transform

The Hilbert transform of a function $u(x)$, $x \in \mathbb{R}$, is defined as follows

$$H(u)(x) = \frac{1}{\pi} \int_{-\infty}^{\infty} \frac{u(s)}{x - s} ds \,. \tag{1.22}$$

Note that $H(x)$ may be viewed as a convolution between $u(x)$ and the so-called "Cauchy kernel" $h(x) = \frac{1}{\pi x}$. Hilbert transform is a transform that have a simple representation of frequency components, and it preserves the positive frequency component and negate the negative frequency component. In addition, it has a relationship with the Fourier transform. Following the discussion in [3, 29], suppose we have two functions

$$\begin{aligned} f(x) &= \int_0^{\infty} [a(t) \cos xt + b(t) \sin xt] dt \\ g(x) &= -\int_0^{\infty} [b(t) \cos xt - a(t) \sin xt] dt \,. \end{aligned}$$

Refer to Section 1.2.1, expansion functions $a(t)$ and $b(t)$ can be expressed as,

$$\begin{aligned} a(t) &= \frac{1}{\pi}\int_{-\infty}^{\infty} f(u)\cos tu\, du \\ &= \frac{1}{2\pi}[\int_{-\infty}^{\infty} f(u)e^{itu}du + \int_{-\infty}^{\infty} f(u)e^{-itu}du] \\ &= \frac{1}{\sqrt{2\pi}}[F(-t) + F(t)]\,, \end{aligned} \tag{1.23}$$

where $F(t)$ is the Fourier transform of $f(t)$. Similarly,

$$b(t) = \frac{1}{i\sqrt{2\pi}}[F(-t) - F(t)]\,. \tag{1.24}$$

Then substitute the result into the expansion of $g(x)$,

$$\begin{aligned} g(x) &= -\frac{1}{\sqrt{2\pi}}\frac{-1}{i}\int_0^{\infty}[F(u) - F(-u)]\cos ux + \frac{1}{\sqrt{2\pi}}\int_0^{\infty}[F(u) + F(-u)]\sin ux \\ &= -\frac{i}{\sqrt{2\pi}}\int_0^{\infty} F(u)[\cos ux + i\sin ux]du + \frac{i}{\sqrt{2\pi}}\int_0^{\infty} F(-u)[\cos ux - i\sin ux]\,du \\ &= -\frac{i}{\sqrt{2\pi}}\int_0^{\infty} F(u)e^{iux}du + \frac{i}{\sqrt{2\pi}}\int_0^{\infty} F(-u)e^{-iux}\,du \\ &= -\frac{i}{\sqrt{2\pi}}\int_{-\infty}^{\infty} F(u)\mathrm{sgn}(u)e^{iux}du\,. \end{aligned} \tag{1.25}$$

Here $\mathrm{sgn}(x)$ function is defined as

$$\mathrm{sgn}(x) = \begin{cases} -1 & x < 0, \\ 1 & x \geq 0. \end{cases} \tag{1.26}$$

Let $G(u)$ be the Fourier transform of $g(x)$, then in the frequency domain Equation (1.25) becomes

$$G(u) = -iF(u)\mathrm{sgn}(u)\,. \tag{1.27}$$

We know the inverse Fourier transform of $-i\mathrm{sgn}(u)$ is $\sqrt{\frac{2}{\pi}}\frac{1}{x}$, therefore we arrive at conclusion that $g(x)$ is the Hilbert transform of $f(x)$ using the Convolution theorem,

$$g(x) = \frac{1}{\pi}\int_{-\infty}^{\infty}\frac{f(s)}{x-s}ds\,. \tag{1.28}$$

From Equation (1.27) we can conclude the relationship between Hilbert transform and Fourier transform. Hilbert transform has the effect of shifting phase of the negative frequency components by $\frac{\pi}{2}$, and positive frequency components by $-\frac{\pi}{2}$. With the help of Hilbert transform, we can transform the signal to a analytical form.

1.4.1 Analytic Signals and Instantaneous Frequency

Hilbert transform can be used to derive the analytic representation of the signal. Specifically,

$$s_a(t) = s(t) + j\hat{s}(t)\,, \tag{1.29}$$

where s_a is the analytic signal, and $\hat{s}(t) = H[s(t)]$ is the Hilbert transform of $s(t)$. We can express analytic form of the signal in the standard polar form as follows,

$$s_a(t) = A(t)e^{j\phi(t)}\,, \tag{1.30}$$

where $A(t)$ is amplitude as a function of time (also called *envelope signal of* $s(t)$), and $\phi(t)$ contains the phase information.

$$\phi(t) = \arctan[\frac{\hat{s}(t)}{s(t)}]\,. \tag{1.31}$$

Bendar and Pierson [3] defines the *instantaneous frequency* f_0 of a signal at time t as follows,

$$f_0(t) = \frac{1}{2\pi}\frac{d\phi(t)}{dt}\,, \tag{1.32}$$

and the *instantaneous angular frequency* of $s(t)$ is defined as

$$\omega(t) = \frac{d\phi(t)}{dt}\,. \tag{1.33}$$

1.4.2 Hilbert Huang Transform (HHT)

To obtain instantaneous frequencies with physical meaning, signals need to obey some restrictions. For instance, signals cannot contain any intermittency, and the frequency components should be well-separated. For multi-components signals, we need to pre-process the signals to separate several parts that is applicable to Hilbert Transform. Empirical mode decomposition (EMD) is proposed by Huang, et al. [18] to solve this problem. The EMD and Hilbert transform are referred as Hilbert-Huang transform (HHT).

HHT provides a novel data-driven method to analyze the non-stationary signals in the time-frequency domain. It has proved its great precision for mono-component signals. Signals will first be decomposed by the EMD into several Intrinsic Mode Functions (IMFs). Then we apply the Hilbert transform to each IMF to calculate the instantaneous frequencies. We can then present the time-frequency analysis result in the Hilbert spectrum. The detail of this algorithm will be introduced in the next chapter.

Chapter 2

Empirical Mode Decomposition

2.1 EMD Introduction

Huang et al. [18] introduced the empirical mode decomposition (EMD) in 1998 as a tool to analyze linear and non-stationary signals. EMD has been applied quite successfully in science and engineering. It treats a signal as a mixture of components and applies a *sifting process* to separate different modes of oscillation which are referred to as Intrinsic Mode Functions (IMF). EMD is essentially a decomposition algorithm that extracts the highest local frequency components from the signal for each IMF. A repeated application produces decomposition of a signal into of components with decreasing frequency. The Hilbert transform is then applied to each component to determine instantaneous frequencies. The results can then be combined to produce a local time-frequency analysis of the signal (Hilbert Spectrum) .

EMD allows us to process transient signals more accurately than Fourier-based methods. Fourier analysis is limited by the uncertainty principle, which means we can only get limited precision on time and frequency. Instantaneous frequency can present the transient signal with precise locality, but the problem of instantaneous frequency is, as shown in the previous chapter, that we can only obtain one single IF value for each time frame. EMD enables us to decompose signals into IMFs, so that we can obtain multiple instantaneous frequencies for different IMFs. Furthermore, EMD provides an alternative approach to the signal analysis. It can adaptively decompose signals and it is able to reveal the physical nature behind it.

2.1.1 Algorithm Description

The details of the EMD algorithm are described below. First of all, we need to detect the local maxima and minima as the local identity of the signal. Then we interpolate the local extrema with a cubic spline, thus, we obtain two curves: upper envelope and lower envelope. By taking the average of these two envelopes, we have the "mean envelope", which can reflect the oscillation of the low frequency components. The mean envelope will be subtracted from the initial signal, and the same process will be repeated on the remainder until it satisfies stop criterion of IMF. This procedure is called "sifting process". The stop criterion of IMF defined in the classic EMD is two-fold [18]:

1. The local mean of the envelopes obtained from local maxima and minima should be zero, implying the IMF is supposed to have zero local mean.
2. The number of local extrema and the number of zero-crossings must differ by at most one.

We will decompose the a signal $s(x)$ into several IMFs by iterating the sifting process. The result is as follows,

$$s(x) = r_k(x) + \sum_{k=1}^{K} \mathrm{IMF}_k(x)\,, \tag{2.1}$$

where $r_k(x)$ represents the residual, and $\mathrm{IMF_k}$ represents the kth order IMF. The classical EMD algorithm may be summarized as follows:

1. Find all local maximal and minimal points of the signal $S(x)$.

2. Interpolate between maximal points to obtain upper envelope function $E_{upper}(x)$ and between minimal points to obtain lower envelope function $E_{lower}(x)$.

3. Compute the mean envelope: $m(x) = \frac{1}{2}(E_{upper}(x) + E_{lower}(x))$.

4. Extract mean from signal: $c(x) = S(x) - m(x)$.

5. If $c(x)$ is not an IMF, iterate Step 3 and 4 until it is.

6. After finding IMF, subtract it from $S(x)$ and repeat Step 2 to obtain the residual.

Figure 2.1 demonstrates how the mean envelope is obtained from the extrema. After obtaining the IMFs, we analyze the IMF by using its Hilbert transform. Recall that

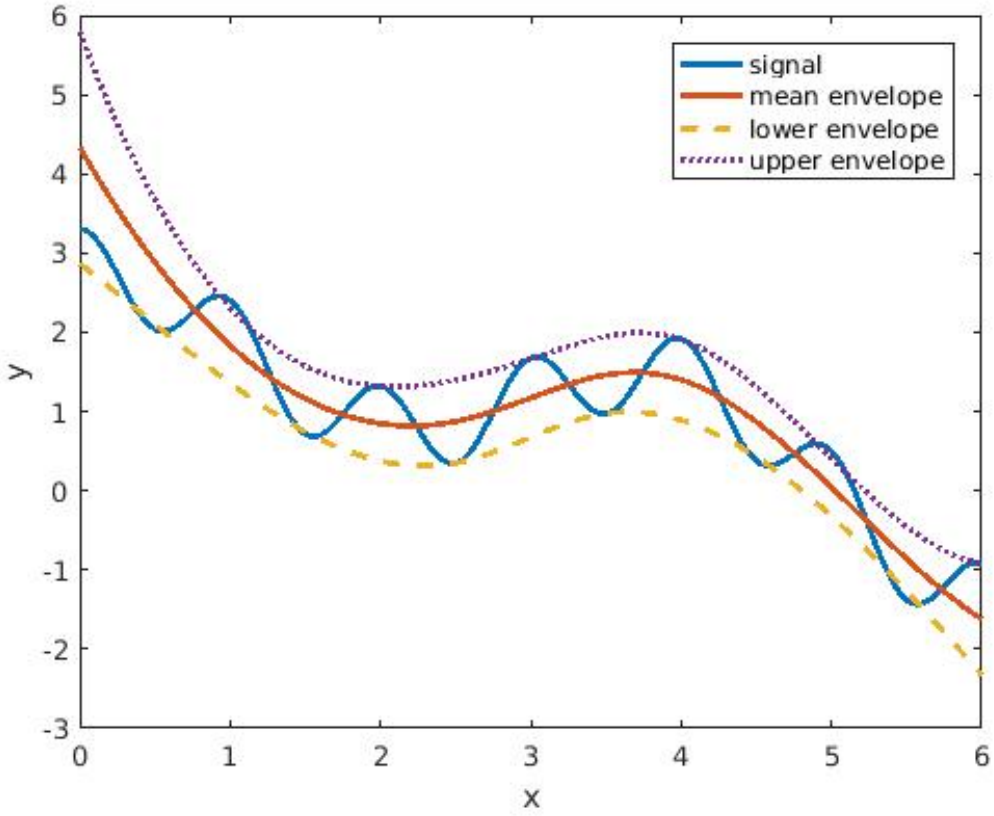

Figure 2.1: Mean envelope demonstration

Hilbert transform on a real function $u(t)$, $H(u)(t)$, is defined as

$$H(u)(t) = \frac{1}{\pi}\int_{-\infty}^{\infty}\frac{u(\tau)}{t-\tau}d\tau, \tag{2.2}$$

With Hilbert transform, we can have the analytic form of the signal $Z(t)$

$$Z(t) = u(t) + iH(u)(t) = A(t)e^{i\theta(t)} \tag{2.3}$$

where

$$\begin{cases} A(t) &= [u^2(t) + H^2(u)(t)]^{1/2} \\ \theta(t) &= \arctan(\frac{H(u)(t)}{u(t)}), \end{cases} \tag{2.4}$$

Refer to Equation (1.33) instantaneous angular frequency is $\omega = \frac{d\theta}{dt}$. For any function to have a meaningful instantaneous frequency, the real part of its Fourier transform has to be a positive frequency. A simple example is a pure tone signal:

$$u(t) = \sin(\omega t). \tag{2.5}$$

Its Hilbert transform is simply $\cos(\omega t)$. So that the analytical form is that

$$Z(t) = \sin(\omega t) + i\cos(\omega t) = e^{i\omega t} \tag{2.6}$$

The instantaneous frequency of this pure tone is $\frac{d(\omega t)}{dt} = \omega$, as expected.

Next step we construct the Hilbert Spectrum(HS) with the instantaneous frequencies [22]. HS will represent the frequency energy distribution as a function of time and frequency $H(l,t)$. To construct the HS, we divide the frequency into L equally spaced bins (L can be anything up to Nyquist limit). The overall HS is expressed as the superposition of the HSs of all the individual IMFs. Hence, every element in $H(l,t)$ is defined as the weighted sum of the instantaneous amplitudes at lth frequency bin, i.e.

$$H(l,t) = \sum_{k=1}^{K} A_k(t)B_k^l(t)\,, \tag{2.7}$$

where K is the number of IMFs, $A_m(t)$ is the instantaneous amplitude of kth IMF, and $B_k^l(t)$ is the weighting factor. $B_k^l(t)$ takes value 1 if the instantaneous frequency falls into the lth frequency bin. After this computation, we will construct the HS $H(l,t)$ as a 2D matrix with same time resolution as the sampling rate and frequency resolution decided by L (up to Nyquist limit).

The marginal Hilbert spectrum is the cumulated frequency energy over the whole time span. It can be calculated by

$$H_{ms} = \sum_{t=1}^{T} H(l,t)\,, \tag{2.8}$$

where T is the time length. Marginal Hilbert spectrum (MHS) is a different spectrum representation compared with Fourier spectrum. As in Fourier transform, energy in frequency bin means there exist a sinusoid; however in MHS, the existence of energy in a particular frequency bin only means that, over the entire data span, there is higher likelihood for such a wave to appear locally.

2.2 Drawbacks/Disadvantages

In application, the frequency analysis tool EMD can adaptively process transient signals. However, it suffers from several problems which need further exploration. In this section we state some of the open problems that exist in EMD method. Our discussion is based partly on the work of Huang [17, 32].

2.2.1 Lack of Mathematical Interpretation

Because most of the work on EMD has focused on algorithms as opposed to mathematical analysis, there has been little work on developing a rigorous theoretical basis for EMD as well as an understanding of why it fails for certain kinds of signals. The need for a mathematical model which explains the principle of EMD and provides a description of the region where it can work effectively has been the motivation for this work. One major obstacle for mathematical modelling of EMD is the interpolation process employed by the algorithm. A rather large number of variables are involved during the interpolation process, and the mathematical expression we obtain during the interpolation is actually piecewise. Since there are multiple intervals between extrema, it is difficult to reveal the mathematical relationship hidden behind the scenes. This, plus the fact that iteration is involved, make it difficult to arrive at an accurate expression in the model.

2.2.2 Vague Definition

The vague definition of IMF brings obstacles in its implementation. In the definition of a IMF, the number of extrema and zero-crossings cannot differ by more than one.

Additionally, the "local mean" of the IMF should be close to zero. The lack of a rigorous definition of IMF makes it difficult to optimize EMD method. Different criteria may generate slightly different sets of IMFs. Moreover, the vague definition makes the sifting process hard to control. We do not know which set of sifting parameters can generate the best IMF set, and we cannot guarantee the uniqueness of IMF. Most of the time, the stopping criterion is chosen empirically, therefore the IMF obtained may vary depending on the parameters. Although such problems exist, they do not affect the analysis considerably, since the results produced by different parameter sets are quite similar.

2.2.3 Boundary Effects

Unavoidably, all data-driven signal analysis methods have boundary effects. In terms of the EMD method, since the interpolation is applied on the global data, interruption of part of the signal can propagate into other parts, and therefore affect the entire output [20]. The the problem is severe when we process short signals.

Proper boundary conditions need to be considered in order to minimize error. Otherwise the mean envelope obtained by EMD is perturbed at the border. If the iteration number is large, the error near the border may be propagated throughout the entire signal. One possible solution is to add a window frame to extend data beyond the existing range [18], so that the interpolation process can extract some information from all the data available. In practice, the extension of data, however, is difficult. Most of the time the signal is non-stationary, and it is difficult to estimate the accuracy of our prediction. Therefore, the problem is still a challenging one, and a satisfactory solution needs further exploration. Figure 2.2 shows the error propagation in the IMF extraction process.

2.2.4 Sampling Effect

In practice signals are discrete, and EMD is generally applied to signals that are "well-sampled" (oversampling). As mentioned in [23], if the sampling rate fs is not sufficiently large, sampling effects will make the analysis much more complicated and cause a loss of accuracy. The natural requirement of sampling is that the discrete signal has to preserve extrema as they play a significant role in EMD algorithm. Suppose the minimal distance between extrema is Δ, then the sampling frequency has to satisfy the condition

$$f_s > 2/\Delta\,. \tag{2.9}$$

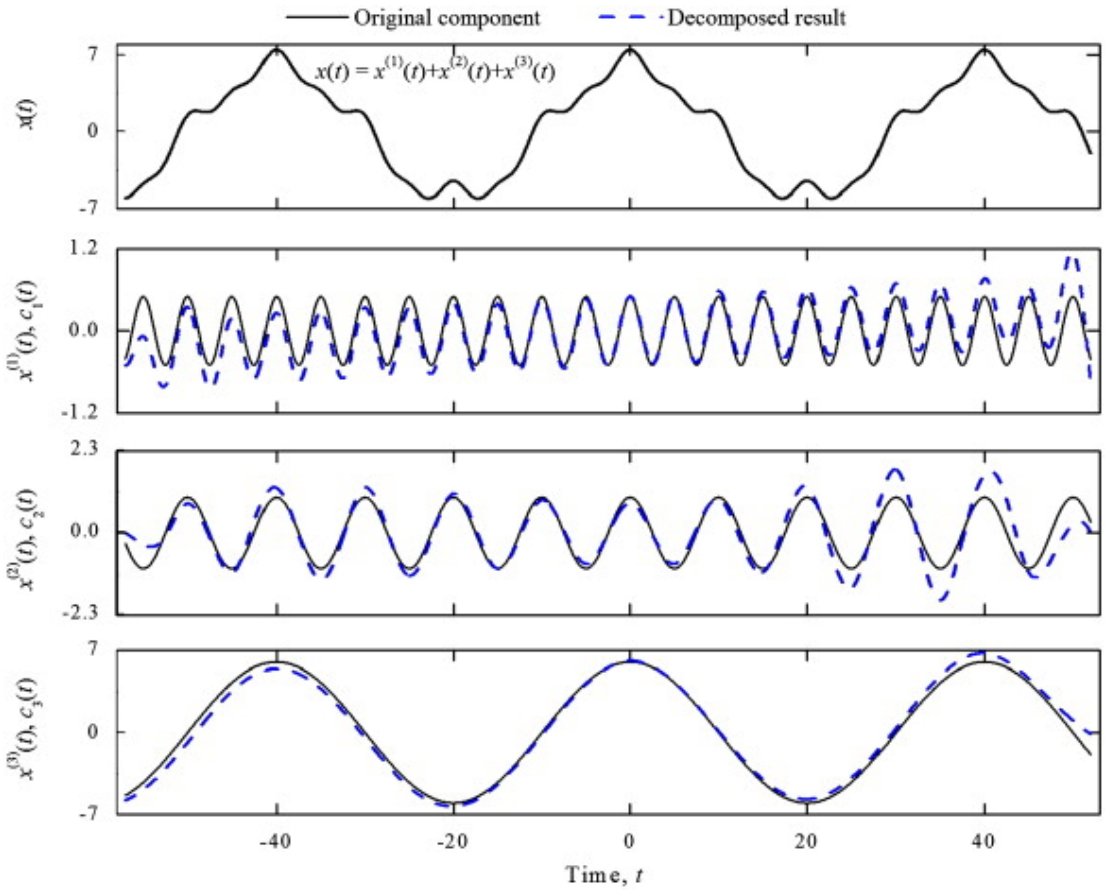

Figure 2.2: EMD decomposition on signal $x(t)$ and its boundary effect. Adapted from "Elimination of end effects in empirical mode decomposition by mirror image coupled with support vector regression", by D. C. Lin and Z. L. Guo and F. P. Ang and F. L. Zeng, 2012, Mechanical Systems and Signal Processing, 31 , p. 13–28. Copyright (2018) by Elsevier. Adapted with permission.

2.2.5 Mode Mixing

There are some kinds of signals, however, for which the sifting process fails to separate into different oscillatory modes. "Mode mixing", a consequence of signal intermittency, first noticed by Huang et al. [32], is one such case. Specifically, portions of signal components are distributed over multiple IMFs. The intermittency contained in the signal can cause serious aliasing in the time-frequency representation, and make the IMF obtained by EMD devoid of physical meaning. Whenever the signal contains riding waves, some frequency components will vanish after performing EMD. This phenomenon results from the interpolation process of the EMD algorithm as it depends on solely extrema. Different frequency components that are concatenated in a piece of signal can have extrema of approximately the same amplitude level, so these different frequency components can be falsely recognized as one in EMD algorithm. Figure 2.3 shows the mode mixing phenomenon that existed in EMD algorithm. To solve this problem, Huang introduced a new method called ensemble empirical mode decomposition (EEMD) [32]. It is using noise-assisted data analysis, which defines the true IMF as the mean of an ensemble of signal adding white noise of finite amplitude. The details of the EEMD method is discussed in Section 5.1.

2.2.6 Frequency Resolution

As studied by Flandrin et al. [25], for combination of two pure tones, the signals relation $af^2 < 1$ is necessary in order to obtain a reasonable decomposition result. Here a and f represent the amplitude and frequency ratios of the corresponding tones. That ratio limits the separation capability of EMD when dealing with different frequency components. Therefore, it is necessary to improve the separation ability so that EMD can have a better resolution for frequency analysis.

2.3 EMD Application and Demonstration

In this section, we will present a demonstration of the EMD algorithm [18] along with the Hilbert spectrum analysis.

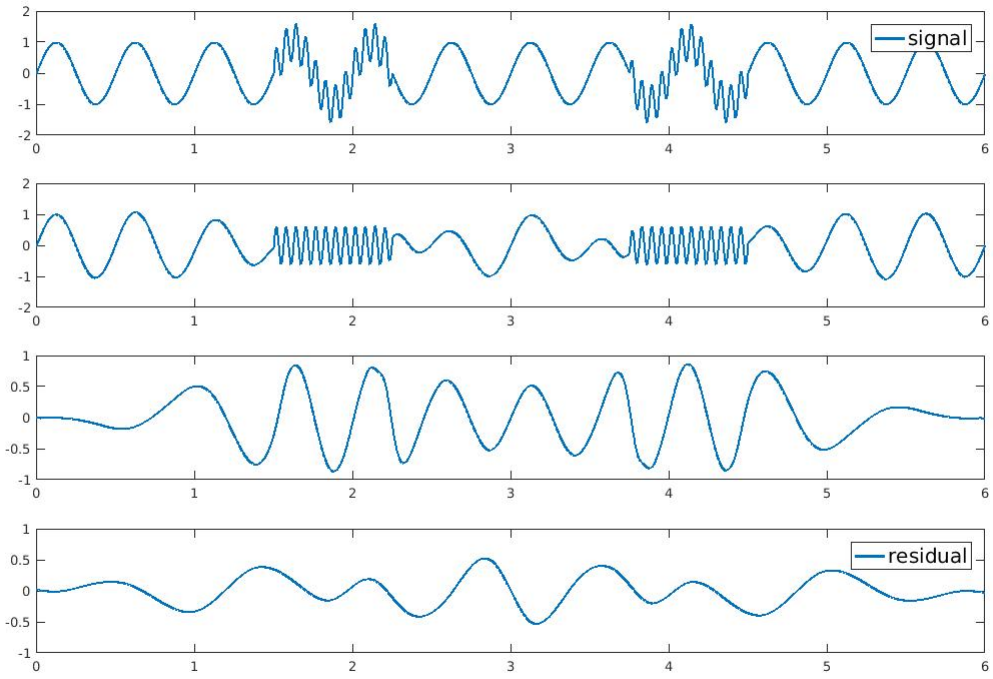

Figure 2.3: Mode-mixing demonstration. From top to bottom are: the signal, IMF1 of the signal, IMF2 of the signal and the residual.

2.3.1 EMD Demonstration on a Synthetic Signal

This example uses a simple synthetic signal that consists of three monotone sinusoids of the expression:

$$x(t) = 0.5\cos(20\pi t) + 2\cos(8\pi t) + 0.8\cos(0.5\pi t) \tag{2.10}$$

It is clear from the Figure 2.4 that EMD decomposes the signal from higher to lower frequency components. The separation ability of the EMD will be discussed in the later chapters using this signal sample.

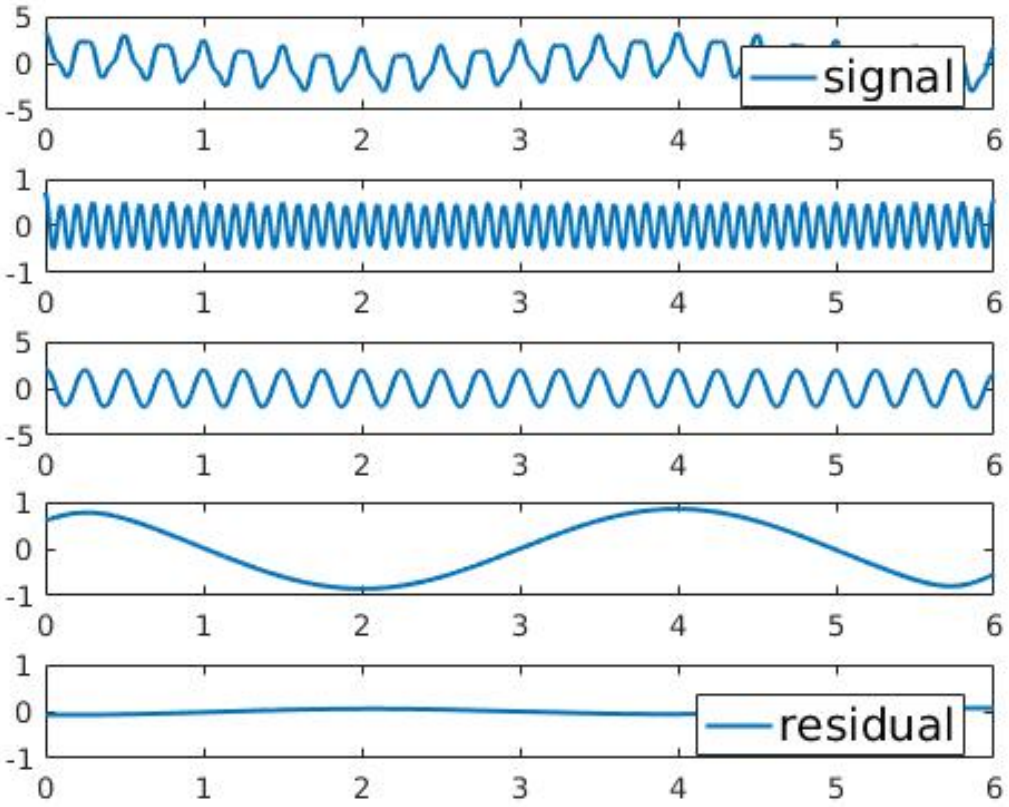

Figure 2.4: IMF demo of three oscillating monotones in Equation (2.10)

2.3.2 Hilbert Spectrum Demonstration

In Figure 2.5, we represent the pure tone (90 Hz with 1kHz sampling rate) by marginal spectra. This figure shows the difference between Fourier and marginal Hilbert spectra. It is apparent that Hilbert spectrum introduce less amount of cross-spectral energy, compared with the STFT based spectra representation. Due to the end effect and frequency leakage phenomenon in Fourier based TF representation, it cannot represent the proper frequency localization. On the contrary, the frequency representation in marginal Hilbert spectrum is still sharp, and define the carrier frequency more clearly. Therefore Hilbert spectrum may better reflect the spatial and frequency information.

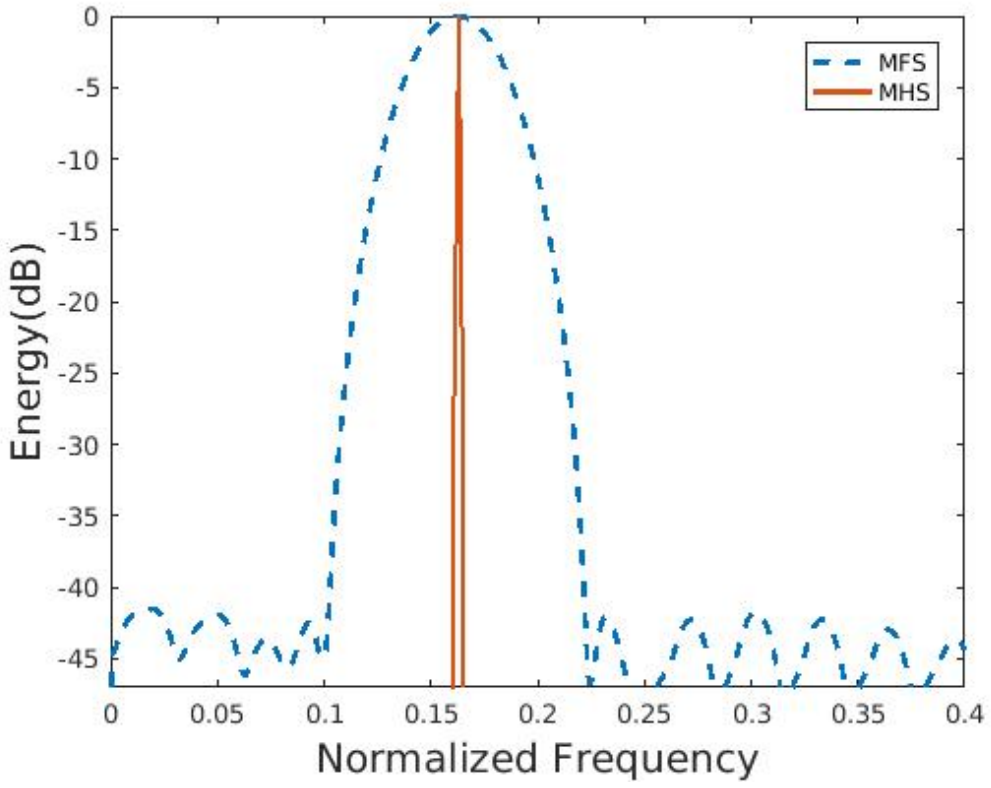

Figure 2.5: Comparison of Marginal Hilbert spectrum (solid line) and STFT (dashed line) based TF representation

2.3.3 EMD Applications

EMD has been widely applied in signal analysis areas, one great example is the application in the field of geophysics, especially when dealing with seismic signals. As it is mentioned in [18] by Huang et al, the Hilbert spectral representation for an earthquake can reveal the physical nature (both linear and nonlinear) of the phenomenon. They showed that Fourier based method underrepresented low-frequency energy for highly non-stationary signal. This is a problem when analyzing the earthquake phenomenon, as seismic waves are definitely non-stationary, and their low-frequency components contain more physics information. By applying the Hilbert-Huang transform, geophysicists can investigate the seismic waves at different scales. They reported success for applying EMD to reflected seismic waves [30] and seismic waves propagation [33].

Other applications include fault diagnosis in rotating machinery [19], short-term wind speed forecasting [31]. Also in the medical field, like EEG seizure detection[2] and EEG synchronization detection[28]. It should be noted that the mentioned examples are only a fraction of the application scenario that EMD can do.

Chapter 3

EMD Related Theoretical Framework

3.1 Backward Heat Equation

As mentioned earlier, interpolation is the major obstacle in the mathematical modelling of EMD. A PDE approach was proposed in [10, 11] to overcome this obstacle. Here, for a prescribed $\delta > 0$, the upper and lower envelopes of a function $h(x)$ are defined as follows,

$$\begin{aligned} U_\delta(x) &= \sup_{|y|<\delta} h(x+y) \\ L_\delta(x) &= \inf_{|y|<\delta} h(x+y)\,. \end{aligned} \tag{3.1}$$

Assume that $h(x)$ is sufficiently differentiable, Taylor expansions are applied to the envelopes so that the mean envelope is defined as

$$m_\delta(x) = \frac{1}{2}(U_\delta(x) + L_\delta(x)) \approx h(x) + \frac{\delta^2}{2}h''(x)\,. \tag{3.2}$$

The sifting process – the process to obtain the Intrinsic Mode Function (IMF) – is then defined as follows,

$$\begin{aligned} h_{n+1}(x) &= h_n(x) - m_\delta(x) \\ h_0(x) &= S(x)\,. \end{aligned} \tag{3.3}$$

For a $\Delta t > 0$, the following Taylor expansion in t is employed,

$$h_{n+1} = h_n(x, t+\Delta t) = h_n + \Delta t\frac{\partial h}{\partial t} + O(\Delta t^2)\,. \tag{3.4}$$

The authors finally arrive at the following PDE,

$$\begin{aligned} &\frac{\partial h}{\partial t} + \frac{1}{\delta^2} h + \frac{1}{2} \frac{\partial^2 h}{\partial x^2} = 0 \\ &h(x, 0) = S(x)\,, \end{aligned} \tag{3.5}$$

which is a *backward heat equation* since the diffusivity constant is negative. (Note that the initial condition, $h(x, 0)$, to this PDE is the original signal $S(x)$.) Unfortunately, there are several drawbacks for this approach:

1. The parameter δ, which is chosen empirically, has a significant influence on the result. For a generalized signal $s = \sum_k A_k \cos(\omega_k x + \phi_k)$, the solution is

$$h(x, T) = \sum_k e^{(\frac{\omega_k^2}{2} - \frac{1}{\delta^2})T} A_k \cos(\omega_k x + \phi_k)\,. \tag{3.6}$$

   As T increases, the amplitudes of components with lower frequencies $\omega < \frac{\sqrt{2}}{\delta}$ will be decreased at each step and therefore vanish at the end of the algorithm. Only the higher frequencies $\omega \geq \frac{\sqrt{2}}{\delta}$ survive. Therefore, choosing δ requires an additional knowledge of the signal.

2. Even if we extract the desired frequency component from the signal, we cannot guarantee that the amplitude of the component is correct. The amplitude of the frequency signals will change according to their frequencies. In order to distinguish two frequency components, one sometimes has to decrease their amplitudes to very small values.

3. As mentioned earlier, Equation (3.5) is a backward heat/diffusion equation. Because the diffusivity parameter is negative, the evolution of a signal will be *opposite* to that of a signal under the standard (forward) diffusion PDE – signals become less smooth and local amplitudes grow exponentially. Especially for sampled signal that is not smooth enough, the backward diffusion equation will cause the signal to lose the physical meaning during the "backward diffusion" process. As expected, numerical methods of this PDE also suffer from instability, and sometimes the output explodes exponentially.

3.2 Long-ranged Diffusion

Interpolation makes it hard to express the sifting process mathematically. As in interpolation, excessive number of variables are introduced, thus making it hard to find their

relationships. In 2005, Niang et al. [9] proposed a new way that tries to solve this problem. They use a fourth-order non-linear equation as the interpolator to simulate the spline interpolation of upper and lower envelope. By controlling the nonlinear terms, the authors use the envelopes obtained by diffusion to replace the ones obtain by interpolation in the classical EMD algorithm. The equation – a long-ranged diffusion (LRD) equation – they use is as follows:

$$\begin{aligned} \frac{\partial h(x,t)}{\partial t} &= \frac{\partial}{\partial x}[g^{\pm}(x,t)\frac{\partial^3 h(x,t)}{\partial x^3}] \\ h(x,0) &= S(x)\,, \end{aligned} \tag{3.7}$$

where $g(x,t)$ is the nonlinear diffusivity function that depends on positions and derivatives (characteristics of extrema). The stopping functions depend on first and second order signal derivatives. The stopping function that selected by the author is

$$g^{\pm}(x) = \frac{1}{3}[|\mathrm{sgn}(\delta_x^1 s_0(x))| \pm \mathrm{sgn}(\delta_x^2 s_0(x) + 1]. \tag{3.8}$$

The sign function is not differentiable, so we need a function to approximate the sign function. A possible expression is given by a regularized version.

$$\mathrm{sgn(z)} = \frac{2}{\pi}\mathrm{arctan}(\pi z/a) \tag{3.9}$$

We know that at extrema, the first derivative is zero, and the second derivative is positive for maxima (negative for minima). The stopping function is designed to use derivatives such that, $g^+(x)$ is set to be zero at maxima, and $g^- = 0$ at minima of the signal. So the PDE solution will diffuse everywhere except on the extrema of the signal. The solution of this fourth-order PDE will converge to the asymptotic solution $s_\infty^+(x)$ (similarly $s_\infty^-(x)$), which is the polynomial interpolation of the successive maxima(or minima) of a signal. Therefore we can replace the interpolation process by this PDE. We can obtain the envelopes by a coupled PDE:

$$\begin{aligned} \frac{\partial h^+(x,t)}{\partial t} &= \frac{\partial}{\partial x}[g^+(x,t)\frac{\partial^3 h^+(x,t)}{\partial x^3}] \\ \frac{\partial h^-(x,t)}{\partial t} &= \frac{\partial}{\partial x}[g^-(x,t)\frac{\partial^3 h^-(x,t)}{\partial x^3}]\,. \end{aligned} \tag{3.10}$$

The asymptotic solutions $h_\infty^+(x)$ and $h_\infty^-(x)$ are the upper and lower envelopes for this method. Therefore the mean envelope here:

$$h_\infty = \frac{1}{2}[h_\infty^+(x) + h_\infty^-(x)]\,. \tag{3.11}$$

The rest of the process is similar to the classic EMD. Mean envelopes are calculated through the proposed PDE, and then are subtracted from the original signals until the residue satisfy the IMF condition. The process will be repeated iteratively until we decompose the signals into numerous IMFs.

3.3 Synchrosqueezed Wavelet

Daubechies [8] proposed an EMD-like wavelet transform as an alternative way to understand the EMD algorithm. The synchrosqueezed wavelet works as a powerful tool for time-frequency representation with solid theory. This method has rigorously expressed the IMFs with clear mathematical expressions. It reveals that only when the signal satisfies certain conditions, the mixture of different frequency components can be separable . This algorithm employs wavelet analysis and reallocation method and provides a precise mathematical expression for a series of separable harmonic components in the signal. The synchrosqueezed method will estimate the FM-demodulated frequency from the wavelet representation before performing reassignment. Essentially, the algorithm is designed to decompose signals into time-varying oscillations. Signal $s(t)$ is assumed to have the general form

$$s(t) = \sum_{k=1}^{K} A_k(t) cos(2\pi\phi_k(t)) + e(t)\,. \tag{3.12}$$

Here $e(t)$ represents the error or the residual. The synchrosqueezed wavelet transform will manage to recover each oscillation component (both the amplitude A_k and the instantaneous frequency $\phi'(k)$). The synchrosqueezed transform mainly consists of three steps [4], First take CWT W_s of the signal $s(t)$, then give an initial estimate of the FM-demodulated frequency by differentiation. Finally, we use that estimate to squeeze W_s via assignment. For the first step we take the CWT,

$$W_s(a,b) = \int s(t) a^{-1/2} \overline{\psi(\frac{t-b}{a})} dt\,, \tag{3.13}$$

where ψ is an appropriately chosen wavelet. Here $W_s(a,b)$ are the coefficients representing the time-frequency spectrum. Following the idea of EMD algorithm, we reallocate the $W_s(a,b)$ to "sharpen" the frequency representation. Take derivative of the wavelet representation to obtain the instantaneous frequency.

$$\omega_s(a,b) = \begin{cases} \frac{-i\partial_b W_s(a,b)}{W_s(a,b)}, & |W_s(a,b)| > 0 \\ \infty, & |W_s(a,b)| = 0\,. \end{cases} \tag{3.14}$$

This transform is called the *synchrosqueezed transform.*

Consider the following simple example of a pure tone harmonic signal

$$s(t) = A\cos(\omega t)\,, \tag{3.15}$$

with the Fourier transform of $\hat{s}(t)$

$$\hat{s}(t) = \pi A[\delta(\xi-\omega)+\delta(\xi+\omega)]\,. \tag{3.16}$$

By Plancherel's Theorem, we can rewrite the CWT of $s(t)$ as :

$$W_s(a,b) = \frac{1}{2\pi}\int \hat{s}(\xi)a^{1/2}\overline{\hat{\phi}(a\xi)}e^{ib\xi}d\xi \tag{3.17}$$

$$= \frac{A}{4\pi}\int [\delta(\xi-\omega)+\delta(\xi+\omega)]a^{1/2}\overline{\hat{\phi}(a\xi)}e^{ib\xi}d\xi \tag{3.18}$$

$$= \frac{A}{4\pi}a^{1/2}\overline{\hat{\phi}(a\omega)}e^{ib\omega}\,, \tag{3.19}$$

where $\hat{\phi}(a\xi)$ is the Fourier transform of $\phi(a\xi)$ The instantaneous frequency $\omega_s(a,b)$ can be computed as the derivative of the CWT at any point (a,b) with respect to b, for all $W_s(a,b)\neq 0$. The result is ω as desired.

$$\omega_s(a,b) = \frac{-i}{W_s(a,b)}\frac{\partial W_s(a,b)}{\partial b} = \omega\,. \tag{3.20}$$

By applying the above transform to every (a,b) points, we obtain the desired information in time-frequency space. Every point (b,a) is converted to $(b,\omega_s(a,b))$. The final step is to reassign energy according to the map $(b,a)\to(\omega_s(a,b),b)$. Follow the inverse CWT we have

$$s(b) = 2R_\psi^{-1}Re(\int_0^\infty W_s(a,b)a^{-3/2})da)\,, \tag{3.21}$$

where $R_\psi^{-1} = \sqrt{2\pi}\int_0^\infty \xi^{-1}\overline{\hat{\psi}(\xi)}d\xi$ is the normalizing parameter. Then we squeeze the frequency representation using the estimate ω_s. Define the frequency divisions such that $\{\omega_l\}_0^\infty$, and $\omega_{l+1}>\omega_l$ for all l. In addition, we define Ω_l as the set of points ω closer to ω_l than to any other ω_l'. The Discrete Wavelet Synchrosqueezed transform of s is then defined as,

$$T_s(\omega_l,b) = \int_{a:\omega_s(a,b)\in\Omega_l} W_s(a,b)a^{-3/2}da\,. \tag{3.22}$$

Chapter 4

Forward Diffusion EMD

In this chapter a novel forward diffusion EMD is proposed as a new theoretical framework for EMD algorithm with the purpose of overcoming the shortcomings of EMD and providing a theoretical analysis at the same time. The modified decomposition method increases the speed of computation. Additionally, the new method can overcome the "mode-mixing" issue that existed in the classical EMD. We present this algorithm in both PDE implementation and convolution implementation, and apply the new method to several typical signals to demonstrate its performance. Finally, we provide some results of this method, along with a comparison of the computational times of different implementations.

4.1 Proposed New Work

Traditionally EMD applies the cubic spline interpolation in the sifting process. These procedures are time-consuming and sensitive to error and noise. It also lacks concise mathematical expressions (the expression is piecewise polynomials). Our new method was proposed based on the backward method mentioned in the previous chapter [10]. It is also proposed to overcome the shortcoming of the backward heat equation (numerical instability) and provide a replacement to the cubic spline. Our method is based on the intuition that the mean curve $m(x)$ should pass through inflection points of the signal. In fact, the Equation (3.2) verifies the intuition. For a signal $h(x)$, when x is a point of inflection the mean curve $m_\delta(x) \approx h(x)$, and the maxima and minima are pushed downwards and upwards, respectively. This motivates an iterative procedure that is simply driven by the second derivative term $h''(x)$. For a prescribed $\tau > 0$, let

$$h_n(x) = h(x, n\tau), \quad n = 0, 1, 2, \dots, \tag{4.1}$$

similarly to backward equation derivation, we then define the iteration procedure,

$$h_{n+1} = h_n + C\frac{\partial^2 h_n}{\partial x^2}\,. \tag{4.2}$$

Now apply the following Taylor expansion to h_{n+1},

$$\begin{aligned} h_{n+1}(x) &= h(x, n\tau + \tau) \\ &= h(x, n\tau) + \tau\frac{\partial h}{\partial t}(x, n\tau) + O(\tau^2) \\ &= h_n(x) + \tau\frac{\partial h_n}{\partial t} + O(\tau^2)\,. \end{aligned} \tag{4.3}$$

Comparing Equation (4.2) and Equation (4.3), we arrive at

$$\tau\frac{\partial h}{\partial t} + O(\tau^2) = C\frac{\partial^2 h}{\partial x^2}\,. \tag{4.4}$$

Now assume $C = a\tau$, divide by τ and let $\tau \to 0$ to obtain

$$\begin{aligned} \frac{\partial h}{\partial t} &= a\frac{\partial^2 h}{\partial x^2} \\ h(x, 0) &= S(x)\,, \end{aligned} \tag{4.5}$$

For prescribed values of the diffusivity constant $a > 0$ and time $T > 0$ (both of which can be adjusted and will be discussed in the later section), we define the *mean function* of $S(x)$ as

$$m(x) = h(x, T)\,, \tag{4.6}$$

which is the solution of the initial value problem in Equation (4.5) at time T. Note that $m(x)$ is equivalent to the convolution of $S(x)$ with the Gaussian function with standard deviation a when S(x) is infinitely long. Figure 4.1 demonstrates the mean envelope extraction in our new method. To further explain this, we refer to the Section 2.1.1, Step 2 and 3. When extracting the envelopes, instead of taking the average of two envelopes, a forward heat equation is introduced to construct a mean envelope. Thus we can avoid the interpolation process in the sifting process. The forward diffusion equation will not lose smoothness during the diffusion process. This mean envelope can be viewed as the result of passing the signal through a smooth filter - in this case, a Gaussian filter. Figure 4.2 is a demonstration of how diffusion will affect the shape of a square wave. The rest of the steps are similar to the classical EMD. After extracting the mean envelope from the signal,

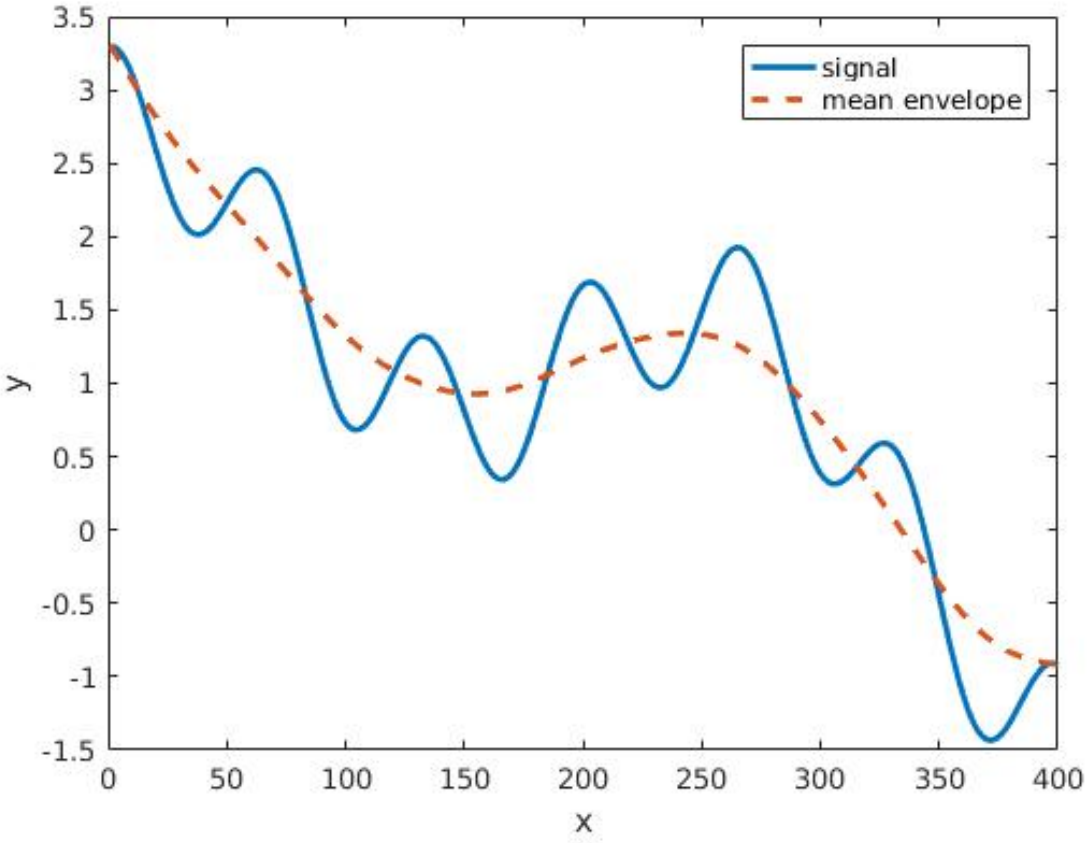

Figure 4.1: Mean Envelope Obtained by Forward Heat Equation

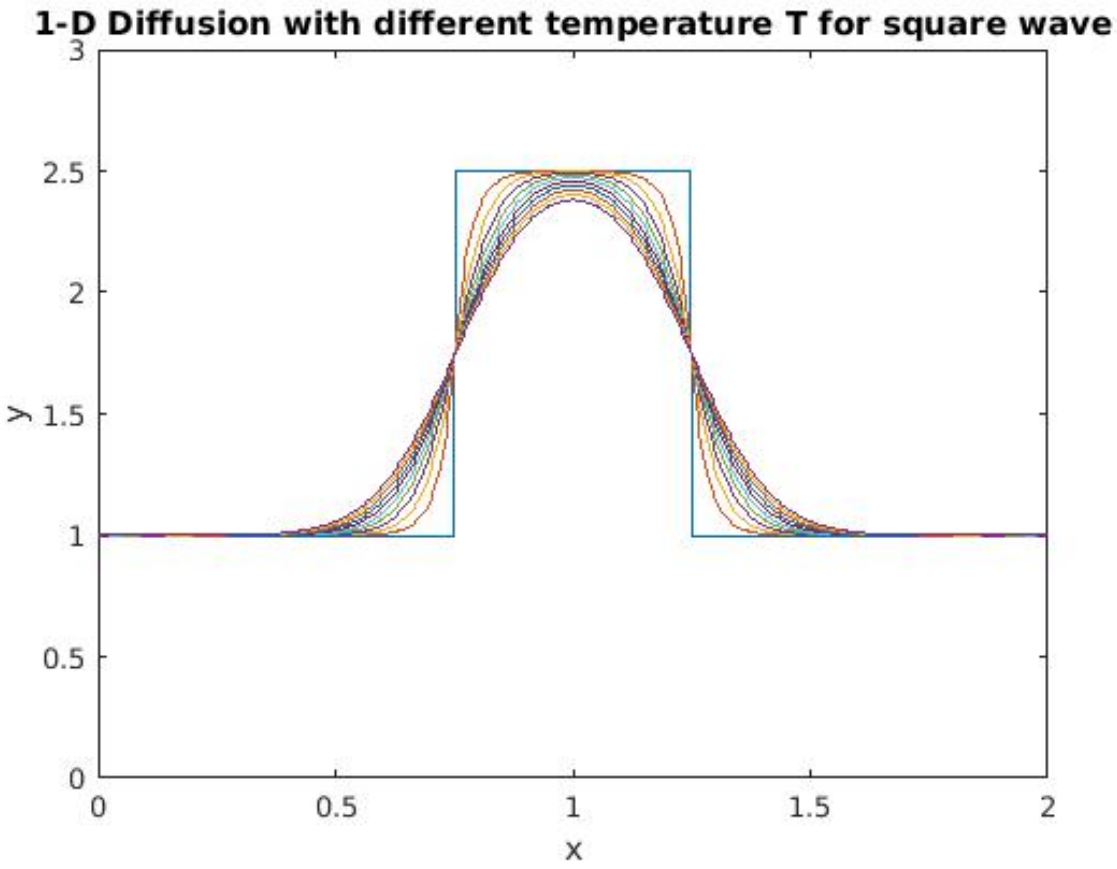

Figure 4.2: Diffusion effect on a square wave with different temperatures

subtract the mean and check whether the result satisfies the IMF condition. Note that in our new method we do not involve the extrema condition when determining IMFs. We will only check the first condition, which states that the mean function should have a zero local mean. . If the result is not a IMF, keep repeating the above process until it is. The same process will be iteratively to the signal, so that the signal will be decomposed into IMFs and residue. The modified algorithm proceeds as follows:

1. Initialize: Let $n = 0$ and set $h_0(x, 0) = S(x)$.

2. Find mean of $h_n(x, 0)$: Solve the PDE in Equation (4.5) for $h_n(x, t)$ for $0 \leq t \leq T$. Then define $m_n(x) = h_n(x, T)$.

3. Extract mean: Define $c_n(x) = h_n(x, 0) - h_n(x, T)$.

4. If c_n is not an IMF, let $h_{n+1}(x, 0) = c_n(x)$, $n \to n + 1$ and go to Step 2.

Our method clearly differs from other EMD algorithms since it bypasses (i) the complicated procedure of extracting local maxima and minima of a signal as well as (ii) the interpolations of these points to obtain upper and lower envelopes. Instead, the mean curve $m(x)$ is obtained directly from the signal by means of smoothing. Unlike the backward heat equation in Equation (3.5), the PDE employed in our EMD procedure is a *forward* heat equation. As it is well known, forward diffusion is numerically more stable than backward diffusion. Niang's fourth-order PDE in Equation (3.7) could be viewed as quite similar to our second-order PDE. However, as a fourth-order diffusion PDE, it will generate significantly more error when dealing with noise in image signals. As such, our second-order PDE should capture the local features of images more effectively.

4.2 Mathematical Explanation of EMD and Its Limitations

4.2.1 Forward PDE Interpretation of EMD

Here we consider the following simple model which is sufficiently general to represent many realistic signals in practice, a signal $S(x)$ consists of numerous sinusoids.

$$\begin{aligned} S(x) &= \sum_{k=1}^{K} A_k \cos(\omega_k x + \phi_k) + C \\ &= \sum_{k=1}^{K} s_k(x) + C\,. \end{aligned} \tag{4.7}$$

Solving Equation (4.5) for first mean envelope PDE, we obtain the expression for mean envelope:

$$m_a(x,T) = \sum_{k=1}^{K} e^{-a\omega_k^2 T} s_k + C \tag{4.8}$$

After N iterations, our modified EMD algorithm yields the following result for the kth cosine component $s_k(x)$,

$$\begin{aligned} h_{k,N} &= (1 - e^{-a\omega_k^2 T}) h_{k,N-1} \\ &= (1 - e^{-a\omega_k^2 T})^N s_k\,. \end{aligned} \tag{4.9}$$

Now suppose, without loss of generality, that $\omega_1 < \omega_2 < \cdots < \omega_K = \omega_{max}$. It is easy to show that for N sufficiently large,

$$\begin{aligned} h_N &= \sum_{k=1}^{K} (1 - e^{-a\omega_k^2 T})^N s_k \\ &\simeq (1 - e^{-a\omega_K^2 T})^N s_K \\ &\simeq s_K\,, \end{aligned} \tag{4.10}$$

where the final approximation is valid for T sufficiently large. By choosing the appropriate set of parameters, the IMF extracted after N iterations will be (at least approximately) the highest-frequency component (HF) s_K. This explains the behavior of the EMD, signals will be decomposed into IMFs that contain frequency components from high to low if we repeat the process.

4.2.2 View of Filter

As stated by Flandrin [12, 13], by experimenting on Gaussian noise and calculate the transfer function, the EMD algorithm is equivalent to a set of filter banks, which is justified in our PDE method. In each iteration of our PDE approach, the mean of the signal is obtained by passing it through a low-pass filter. Subsequent subtraction of the mean from the signal is therefore equivalent to passing it through a high-pass filter.

4.3 Parameter Selection

4.3.1 How to Choose Parameter a

Parameter a is crucial when determining the mean envelope so it must be carefully chosen. It controls how far we want to diffuse the signal. We want the "mean curve" obtained by diffusion to be close to the "mean curve" obtained by extrema. We want to ensure that the mean envelope is always within the range of the signal amplitude. Without loss of generality, we consider a pure tone of unit amplitude $s(x) = \cos(\omega x)$. Solving PDE in Equation (4.5) yields the envelope

$$m(x) = -a\omega^2 \cos(\omega x)\,.$$

To converge, it is necessary that $a \leq \frac{1}{\omega^2}$. As mentioned in [23], if the sampling rate f_s is not sufficiently large, sampling effects will cause a loss of accuracy. We must assume that f_{max}, the maximum frequency to be extracted, satisfies $f_{max} < \frac{1}{2} f_s$. This implies that $\frac{1}{\pi^2 f_s^2} < \frac{1}{\omega_{max}^2}$. It is then safe to set $a = \frac{1}{\pi^2 f_s^2}$. Ideally the parameter a should be set to $a = \frac{1}{\omega_{max}^2}$. There are two practical approach to estimate a:

1. Autocorrelation: The equation of autocorrelation for a discrete signal is

$$R_{yy}(l) = \sum_{n \in z} y(n)\bar{y}(n-l) \tag{4.11}$$

   Calculate the autocorrelation of the signal, and then use the result to estimate the highest frequency component within the signal.

2. Zero-crossing rate: Use zero-crossing rate to estimate the parameter a. Suppose the shortest distance between zeros crossings is L for the signal, then we estimate the

maximal frequency to be

$$a = \frac{1}{\omega_{max}^2} = \frac{1}{4\pi f_{max}^2} = \frac{(2L)^2}{4\pi^2} \tag{4.12}$$

$$= \frac{L^2}{\pi^2}\,. \tag{4.13}$$

Of course, without prior information, these approaches can only provide an approximation to our parameter selection. But for most of the signals that contain limited number of frequency components, these two approaches can generate reasonable results.

4.3.2 Performance Measure of the Separation Ability

As shown in [25], the capability of separation for EMD algorithm is limited. By applying EMD to mixtures of two cosine signals, we can examine the separation capability for different frequency component ratios. Consider a signal composed of two tones:

$$S(x) = s_1(x) + s_2(x)\,, \tag{4.14}$$

where

$$s_1(x) = \cos(2\pi x) \tag{4.15}$$

$$s_2(x) = \alpha\cos(2\pi f x)\,, \tag{4.16}$$

and here α is the amplitude ratio and $\alpha \in (10^{-2}, 10^2)$ and f is the frequency ratio, with the range $f \in (0, 1)$. We use the following performance measure for separation capability:

$$PM = \frac{||\mathrm{IMF}_1 - \cos(2\pi x)||_2}{||\cos(2\pi x)||_2}\,. \tag{4.17}$$

Here IMF_1 represents the first IMF extracted by the algorithm. A perfect separation yields $PM = 0$ as the first IMF is the highest frequency component $\cos(2\pi x)$. In general, the smaller the performance measure, the better is the signal decomposition quality.

The results are presented in Figure 4.3. It should be noted that the performance of our PDE approach is similar to that of the classical EMD method. Our new proposed method still has the difficulty extracting two closely spaced frequency components when the lower frequency component dominates in the signal. A natural solution (compensation) to this problem is to attenuate the lower frequency component, so that two tones will have comparable amplitudes and can be separated by the EMD-based method. On the other hand, if one tone dominates the other, it is acceptable for us to ignore the one with relatively low amplitude, as we can regard it as the noise of the signal.

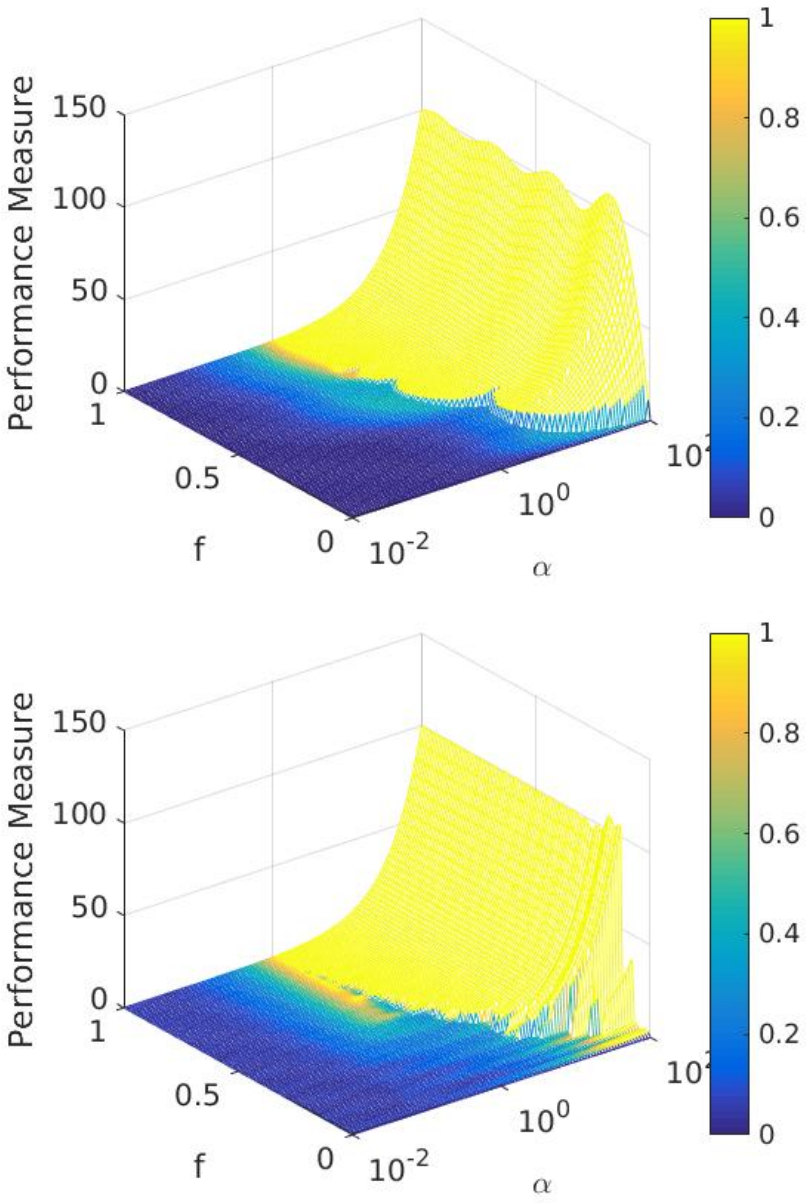

Figure 4.3: Top: Performance Measure Regarding α and f for classical EMD. Bottom: Performance Measure Regarding α and f for forward-PDE approach.

4.3.3 The Pair of Parameters T and N

The parameters a and T determine the shape of the mean curve, and N represents the number of iterations. As shown in Section 4.3.2, the frequency resolution depends on the separation capability of the algorithm. In order to control the separation performance of our algorithm, we impose the variable δ to represents the amplitude ratio between the target frequency component and undesired frequency component. Suppose our target is the frequency component with angular frequency ω, and the undesired component is the one with $r\omega$, where $0 < r < 1$ denotes the ratio between two frequency components (lower/higher). Refer to Equation (4.9), after being decomposed by our algorithm, δ can be expressed as follows,

$$\delta = \left[\frac{1 - e^{-ar^2\omega^2 T}}{1 - e^{-a\omega^2 T}} \right]^N . \tag{4.18}$$

Assume that $e^{-a\omega^2} = \epsilon$, where ϵ should be a value close to zero. δ can be simplified as,

$$\delta = \left[\frac{1 - \epsilon^{r^2 T}}{1 - \epsilon^T} \right]^N . \tag{4.19}$$

and we aim to adjust our parameter set T, N such that (i) δ is close to zero (meaning we can separate the desired target frequency component). (ii) r should be close to 1 (meaning we can separate the target even the two frequency components are very close).

We define r_0 as the *cutoff-frequency ratio*: the algorithm may fail to separate the components $r > r_0$, i.e. if the two components are too close to each other. When $r < r_0$, the ratio of the norms of the lower- and higher-frequency components will satisfy $||\frac{S_{lower}}{S_{higher}}|| < \delta$, i.e. the frequency components are separable. With the restrictions $\delta \approx 0$ and $\epsilon \approx 0$, we can assume $\delta = \epsilon$, and finding the optimal parameters reduces to the following problem,

$$r_0^2 = \left[\frac{\log(1 - \epsilon^{\frac{1}{N}}(1 - \epsilon^T))}{\log \epsilon} \right] . \tag{4.20}$$

Here we seek to maximize r_0. The results of one numerical experiment, with $N = 100.0$ and $T = 10.0$, are shown in Figure 4.4. We can conclude from the figure that for this particular parameter set, theoretical cutoff-frequency ratio should be $r_0 \simeq 0.7$. If we want to increase the cutoff-frequency ratio (to 0.9 for example), we can choose parameters set to be $N = 4000.0\,, T = 15.0$, but this will increase the computational cost considerably. Figure 4.4 provides a guidance when selecting the parameter set T and N. In order to obtain really

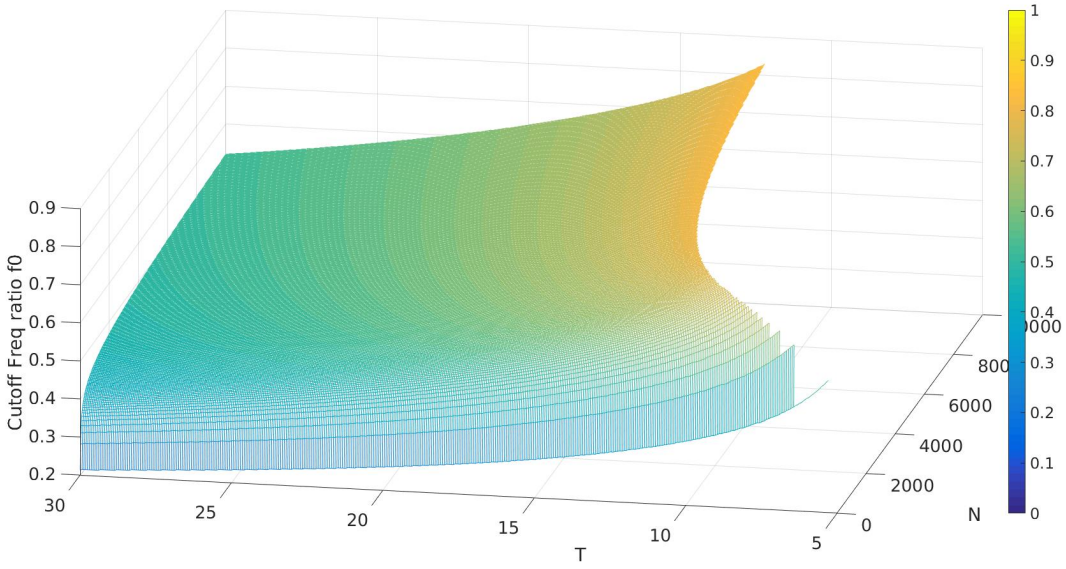

Figure 4.4: cutoff-frequency ratio r_0 with various parameter values T and N

high cutoff-frequency ratio (which means strong separation capability), the product of T and N needs to be big enough; however, the corresponding computational cost will increase. Therefore, there is a trade-off between decomposition quality and the computational cost when choosing the parameters. The parameter set should vary according to our needs.

4.4 Numerical Results

4.4.1 PDE implementation Scheme

The diffusion process is implemented by the explicit finite difference scheme.

$$\frac{u_j^{n+1} - u_j^n}{\Delta t} = a\left(\frac{u_{j+1}^n - 2u_j^n + u_{j-1}^n}{\Delta x^2}\right). \tag{4.21}$$

We use the simplest computational method – the Forward Euler scheme – a forward difference at time t_n and a second order central difference at position x_j . In order to guarantee a reasonable mean envelope shape, we introduce the Neumann boundary condition to this

PDE solver, with zero derivative at both boundaries.

$$\begin{aligned} u'(x_l, 0) &= 0 \\ u'(x_r, 0) &= 0\,. \end{aligned} \tag{4.22}$$

Here x_l and x_r represent the left and right end points, respectively.

4.4.2 Convolution Equivalence

Since we are solving a diffusion equation, it is possible to use a convolution to replace the finite difference/finite element approach. In fact, this method is preferred since it is computationally faster. For infinite long signal, the forward diffusion equation is equivalent to a Gaussian Convolution. For a function $u(x,t)$, the diffusion can be written as:

$$\begin{aligned} \frac{\partial u}{\partial t} &= a\frac{\partial^2 u}{\partial x^2} \\ u(x,0) &= f(x), \quad \text{for} -\infty < x < \infty,\ 0 < t < \infty\,. \end{aligned} \tag{4.23}$$

To solve this equation, we regard $u(x,t)$ as a function of x and do the Fourier transform. The result is a function $U(s,t)$ that depends on the wave number s and time t. In the Fourier domain, the diffusion equation becomes,

$$\frac{\partial U}{\partial t} = a\frac{\partial^2 U}{\partial x^2} \tag{4.24}$$

We know that based on the properties of Fourier transform

$$\frac{\partial^2 U}{\partial x^2} = -4\pi^2\omega^2 U\,, \tag{4.25}$$

and substitute into Equation (4.24),

$$\frac{\partial U}{\partial t} = -4a\pi^2\omega^2 U\,, \tag{4.26}$$

and we have the initial condition when $t = 0$, $U(s,0) = F(s)$. $F(s)$ is the Fourier transform of $f(t)$. Thus, we have

$$U(s,t) = F(s)e^{-4a\pi^2 s^2 t}\,. \tag{4.27}$$

This solution can be written as the convolution of two functions. If we have a function $w_t(x)$ such that its Fourier transform satisfies $W_t(s) = e^{-4a\pi^2 s^2 t}$, then

$$u(x,t) = (f * w_t)(x)\,. \tag{4.28}$$

Here the $w_t(x) = \frac{1}{\sqrt{4\pi at}} e^{-\frac{x^2}{4at}}$ is the Gaussian kernel. Since we are solving a diffusion equation, it is possible to use a convolution to replace the finite difference / finite element approach (much faster). As for infinite long signal, the solution is equivalent to a convolution with a Gaussian function.

$$m_a(x) = \frac{1}{\sqrt{4\pi at}} e^{-\frac{x^2}{4at}} * u(x, 0)\,. \tag{4.29}$$

Convolution implementation can also carry the boundary condition of the PDE. The "symmetric" scheme convolution, i.e. convolution padded with mirror reflections of itself. is equivalent to the forward PDE with zero-derivate Neumann boundary condition. The "replicate" scheme convolution, i.e. convolution padded by repeating border elements of array, is equivalent to the forward PDE with Dirichlet boundary condition.

4.4.3 Two-mode Mixing

This experiment addresses the mode-mixing separation problem. The signal $s(x)$ with length L is built by concatenating two sinusoids with different frequencies,

$$s(x) = \begin{cases} 0.6\sin(2\pi 2x), & 0 < x < L/2 \\ 1.0\sin(2\pi 12x), & L/2 < x < L \end{cases}$$

as shown in Figures 4.5 to 4.7, the signal and its Hilbert spectrum are displayed. It is clear that unlike classical EMD, the forward-PDE approach can distinguish the two modes and produce a reasonable separation. The corresponding Hilbert frequency spectrum can represent the frequency change correctly. As such, it can extract features from mode-mixed signals and obtain better instantaneous frequency details. Classical EMD, however, fails to separate these different modes. Due to the extrema-based nature of classic EMD, for two modes with different frequencies but same amplitude, the classic EMD will treat two modes as just one single frequency component.

4.4.4 Nonlinear Oscillations

Although we have proved our method's capability when dealing with sinusoid-like signals, it remains to be shown that our method can separate the nonlinear oscillations like the EMD does. Figure 4.8 shows a nonlinear signals, we apply our method on the nonlinear

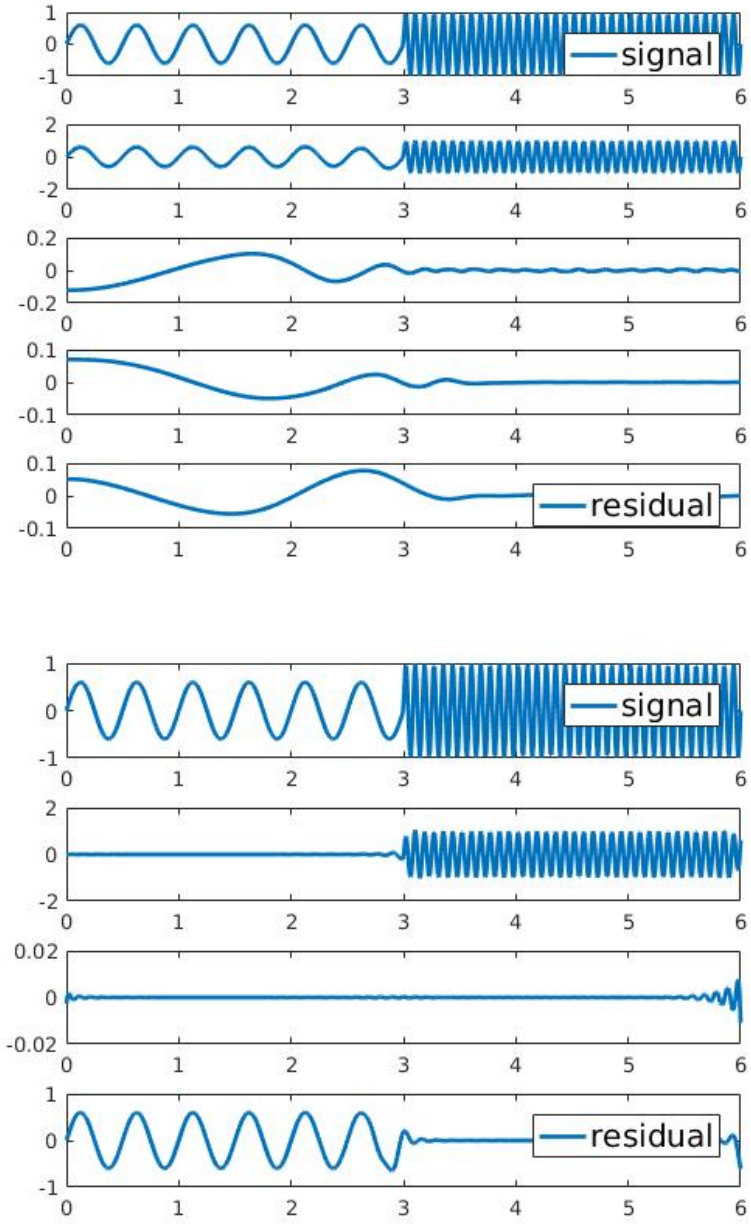

Figure 4.5: Experiment on mode-mixing signal by classical EMD (Top) and forward-PDE approach (bottom)

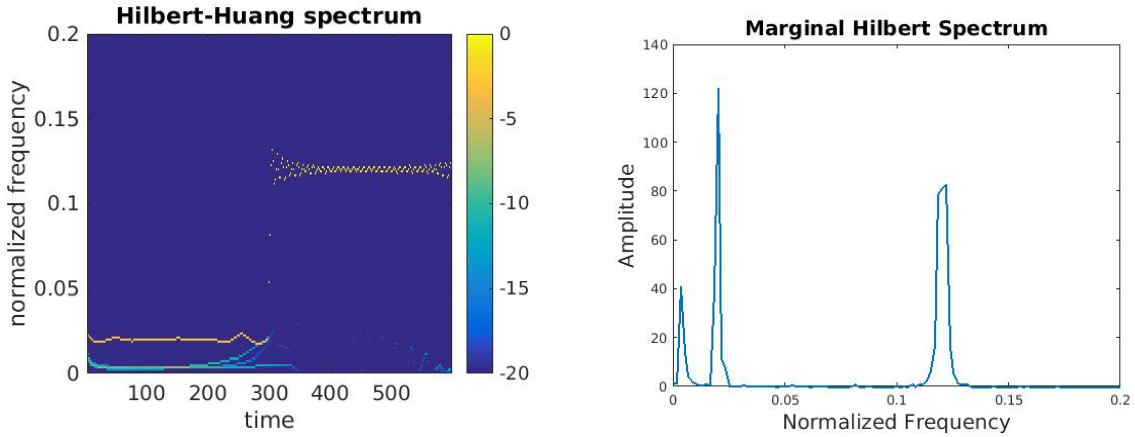

Figure 4.6: Hilbert Spectrum (left) and Marginal Hilbert Spectrum (right) for mode-mixing signal using classical EMD approach.

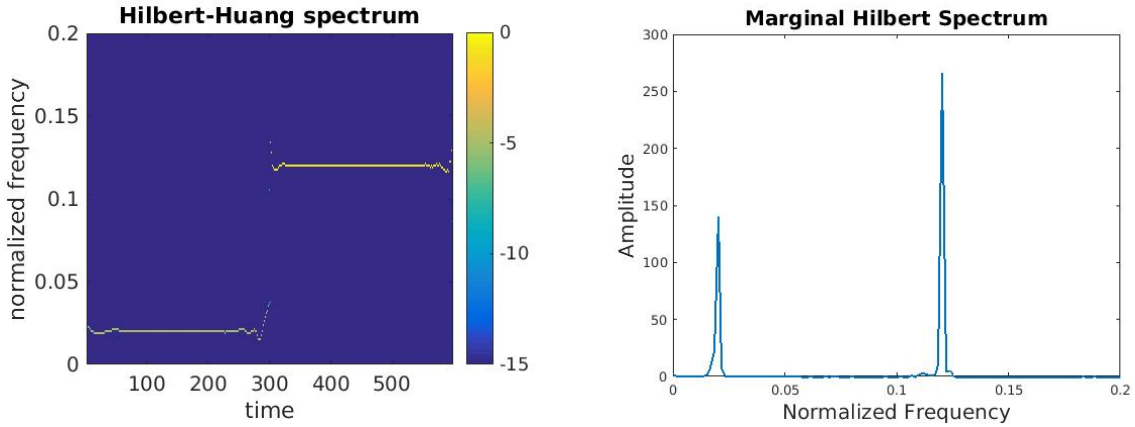

Figure 4.7: Hilbert Spectrum (left) and Marginal Hilbert Spectrum (right) for mode-mixing signal using forward-PDE approach.

signal mentioned in [26] and obtain similar results. The nonlinear signal is composed of three components, a sinusoid of period T superimposed to 2 triangular signals with periods smaller and larger than T,

$$s(x) = \sin(0.06\pi x) + 0.4(1 - 10|\text{nint}(1/5x) - 1/5x|) + 0.4(1 - 352|\text{nint}(1/176x) - 1/176x|)\,, \tag{4.30}$$

where nint is the nearest integer function.

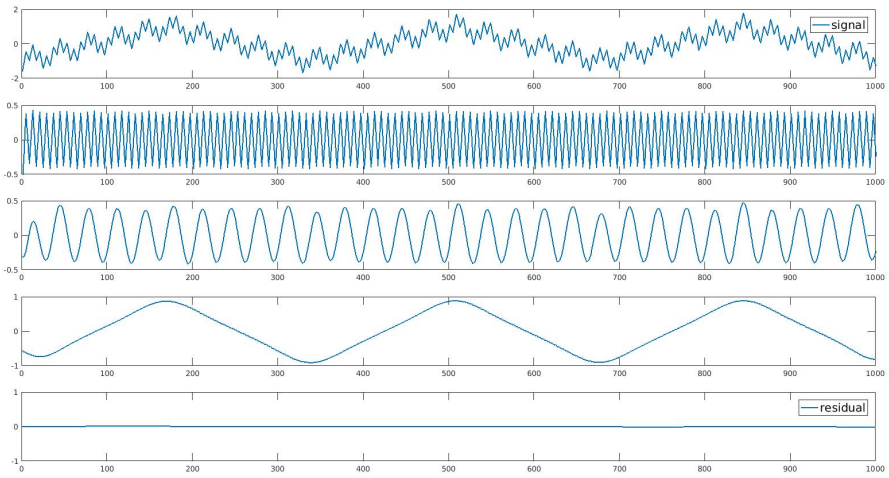

Figure 4.8: Nonlinear oscillations experiment. From top to bottom: the signal, IMF 1 to 3 and the residual.

4.4.5 ECG Signal

In Figure 4.10, we use an electrocardiogram(ECG) signal to test the robustness of forward PDE approach. The data is obtained from MIT-BIH Normal Sinus Rhythm [14]. The decomposition of ECG signal has shown that though the PDE approach can detect the mode, it is not robust to noise.

4.4.6 Computational Time Comparison

In this section, we compare the computational time of the classic EMD and our new method. For our method, we provide the results of two different implementations: PDE

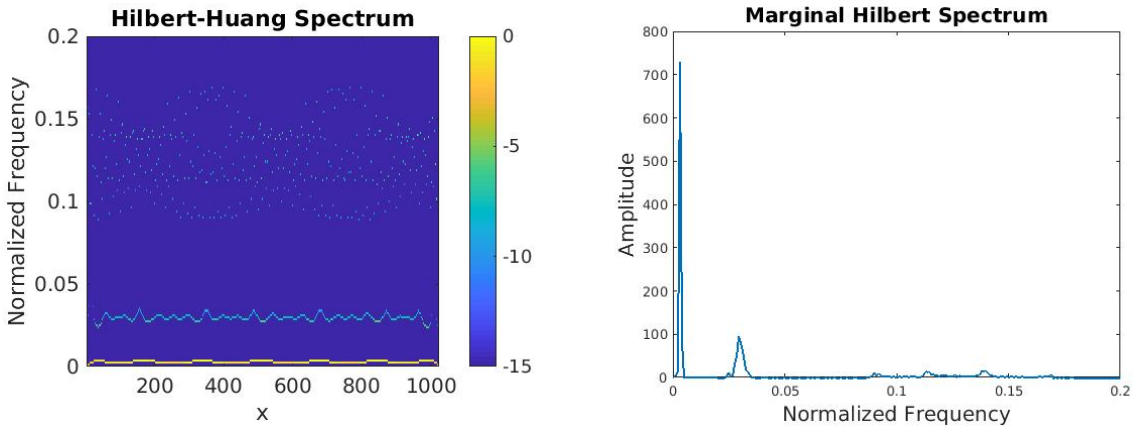

Figure 4.9: Hilbert Spectrum (left) and Marginal Hilbert Spectrum (right) for nonlinear oscillation experiment.

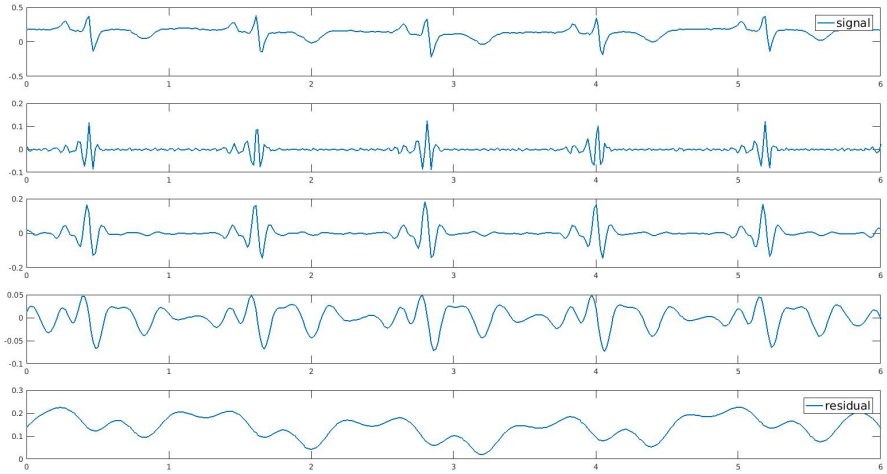

Figure 4.10: Experiment on ECG data. From top to bottom: the signal, IMF 1 to 3 and the residual.

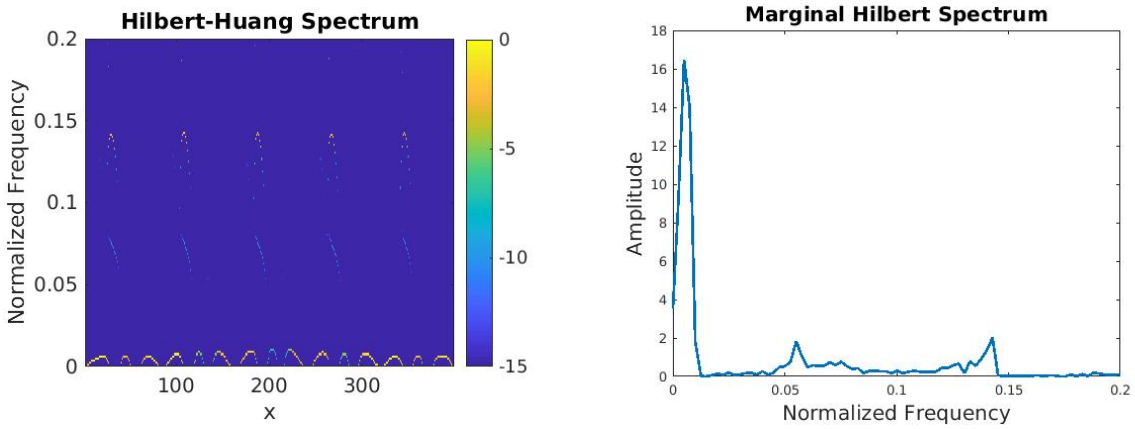

Figure 4.11: Hilbert Spectrum (left) and Marginal Hilbert Spectrum (right) for ECG signal.

and Gaussian convolution.

Traditional EMD methods rely on finding local maxima and minima along with interpolation to find upper and lower envelope. This is computationally expensive. Recall that these procedures are bypassed in our PDE-based approach and replaced by a simple diffusion procedure. As such, our method could potentially require less computational time. To test this conjecture, we have determined the computational times required for a number of iterations of the sifting process for the classical BEMD method as well as our PDE-based BEMD method. (The code based on Flandrin's toolbox [24] was implemented for the classical BEMD method.) The results that obtained by experimenting on a piece of piano signal, presented in the first two columns of Table 4.1, show that our diffusion-based method can decompose a given piece of signal into its IMFs much faster than traditional EMD.

	Trad. EMD	**PDE-based EMD**	**PDE EMD with GC**
1 IMF	0.09445s	0.01776s	0.01692s
2 IMFs	0.16419s	0.02238s	0.01169s
3 IMFs	0.24388s	0.03807s	0.01277s
4 IMFs	0.32565s	0.04747s	0.01047s
5 IMFs	0.40616s	0.05584s	0.01334s

Table 4.1: Comparison of computational times for (i) traditional EMD, (ii) diffusion-based EMD and (iii) diffusion-based EMD using Gaussian convolution (GC) in terms of total number of IMFs computed

4.4.7 Music Signal

In Figures 4.12, 4.14, 4.16 and 4.18, we display the decomposition results of our method on music signals. By sequence, we experiment on piano, oboe and flute signals. Music has relatively fewer harmonic components, so that the decomposition results can display different levels of harmonic structure within the signal pieces.

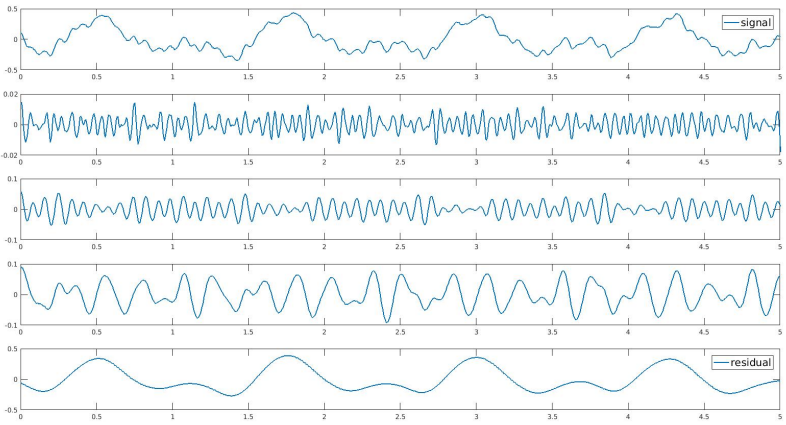

Figure 4.12: Experiment on piano signal. From top to bottom: the signal, IMF 1 to 3 and the residual.

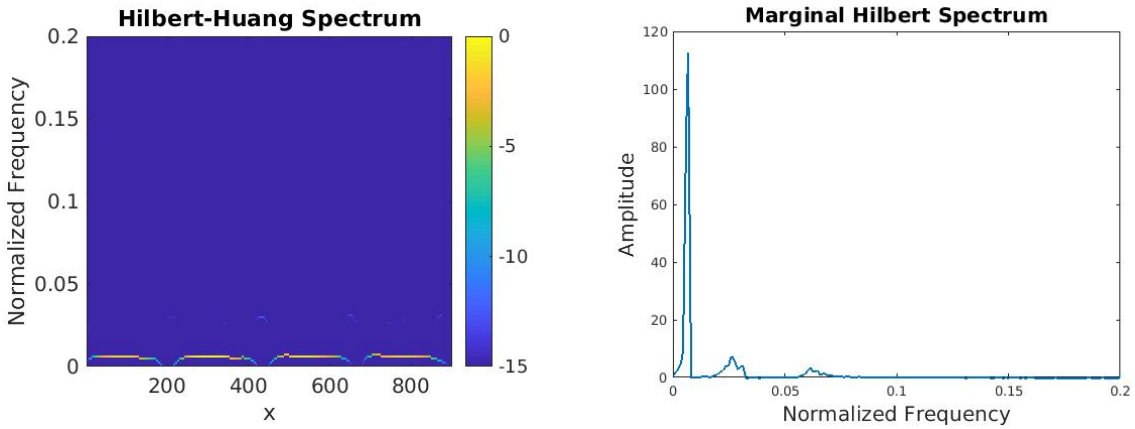

Figure 4.13: Hilbert Spectrum (left) and Marginal Hilbert Spectrum (right) for the piano signal.

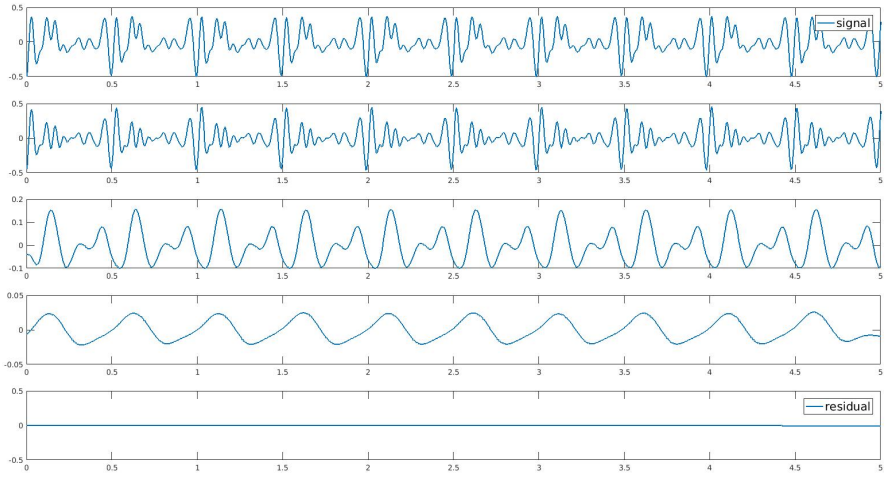

Figure 4.14: Experiment on oboe signal. From top to bottom: the signal, IMF 1 to 3 and the residual.

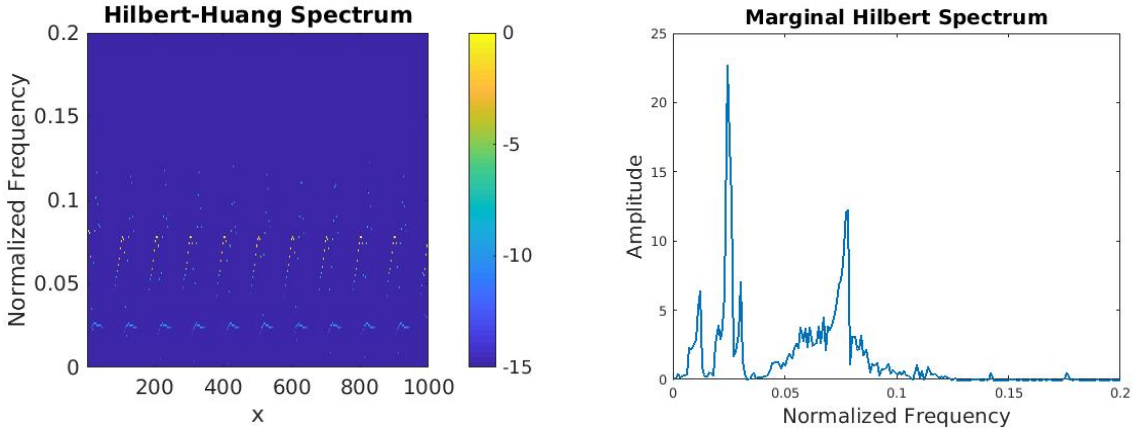

Figure 4.15: Hilbert Spectrum (left) and Marginal Hilbert Spectrum (right) for the oboe signal.

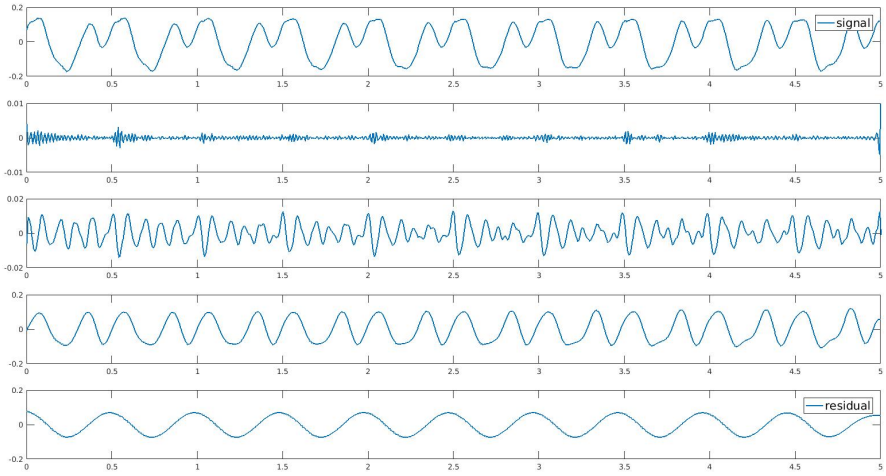

Figure 4.16: Experiment on flute signal. From top to bottom: the signal, IMF 1 to 3 and the residual.

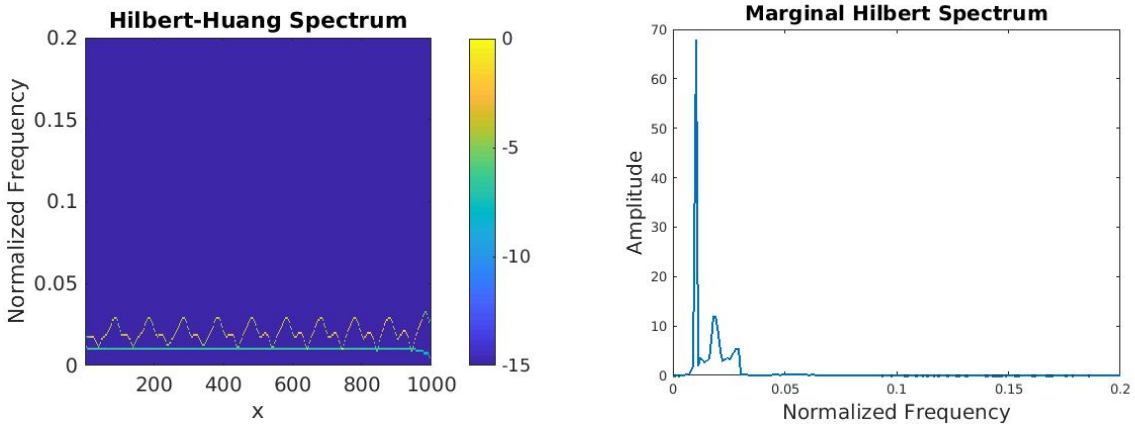

Figure 4.17: Hilbert Spectrum (left) and Marginal Hilbert Spectrum (right) for flute signal.

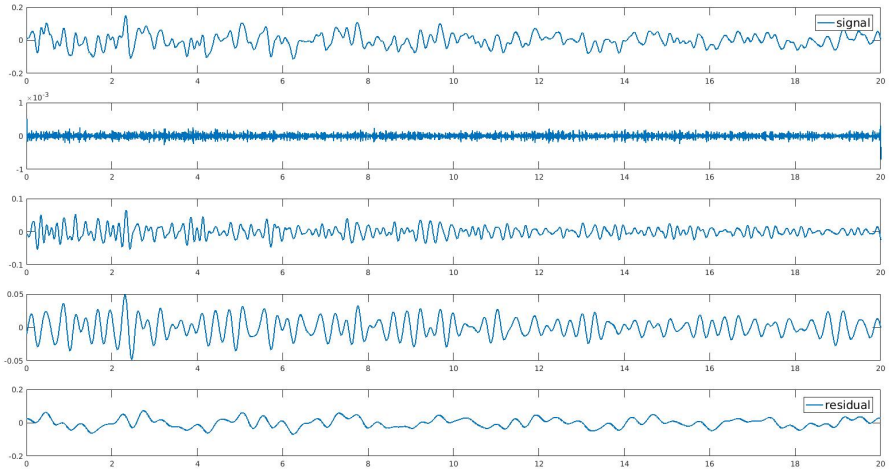

Figure 4.18: Experiment on bendir signal. From top to bottom: the signal, IMF 1 to 3 and the residual.

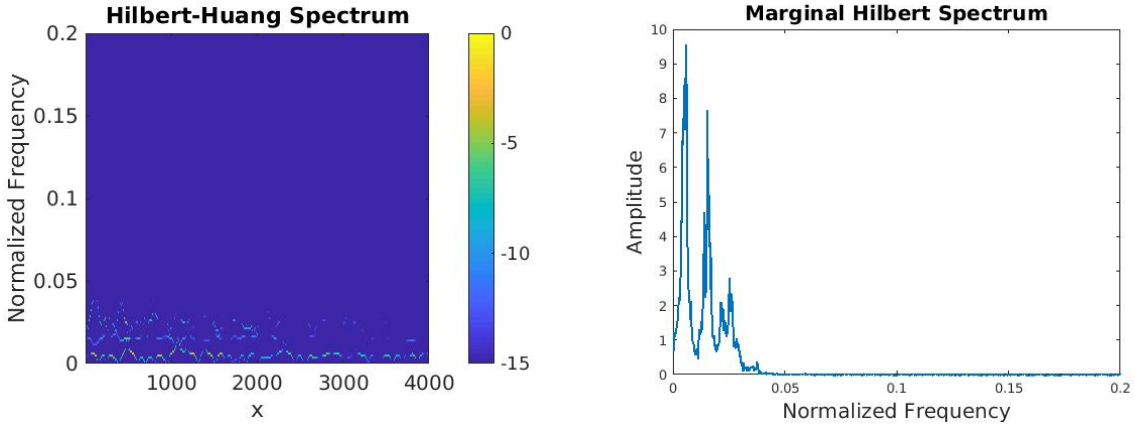

Figure 4.19: Hilbert Spectrum (left) and Marginal Hilbert Spectrum (right) for the bendir signal.

Chapter 5

EMD Extension

There are various extensions to the classical EMD method. Some try to overcome the shortcomings of the EMD methods, and some try to extend the EMD to multi-dimensional cases. Here we select three representative methods and present a brief introduction for each of them.

5.1 Ensemble Empirical Mode Decomposition

As it is mentioned in Section 2.3.5, EMD fails to decompose signal when there is "mode-mixing". Ensemble Empirical Mode Decomposition (EEMD) was proposed to solve this problem. EEMD was developed by Huang et al. [32], and they utilize the noise to help assist the data analysis in the decomposition of EMD. They added white noise to the signal, since white noise can fill whole time-frequency space uniformly. With uniformly distributed white noise background, different frequency components within the signal are projected onto the reference of white noise frequency components. Although it is apparent that adding noise will cause the decomposition results to consist of noise, we can decrease or even cancel the noises by applying white noise for numerous trials. Each trial will produce different results, and statistically, by taking the ensemble mean of enough trials, the noises will cancel out. IMFs in EEMD are defined as the mean of white noise ensembles. This way we can get the persistent decomposition result from the ensemble, and we can significantly reduce the change of mode mixing problem within EMD. Therefore EEMD is more robust to the noise. Figure 5.1 is a comparison of the decomposition results of classic EMD and EEMD.

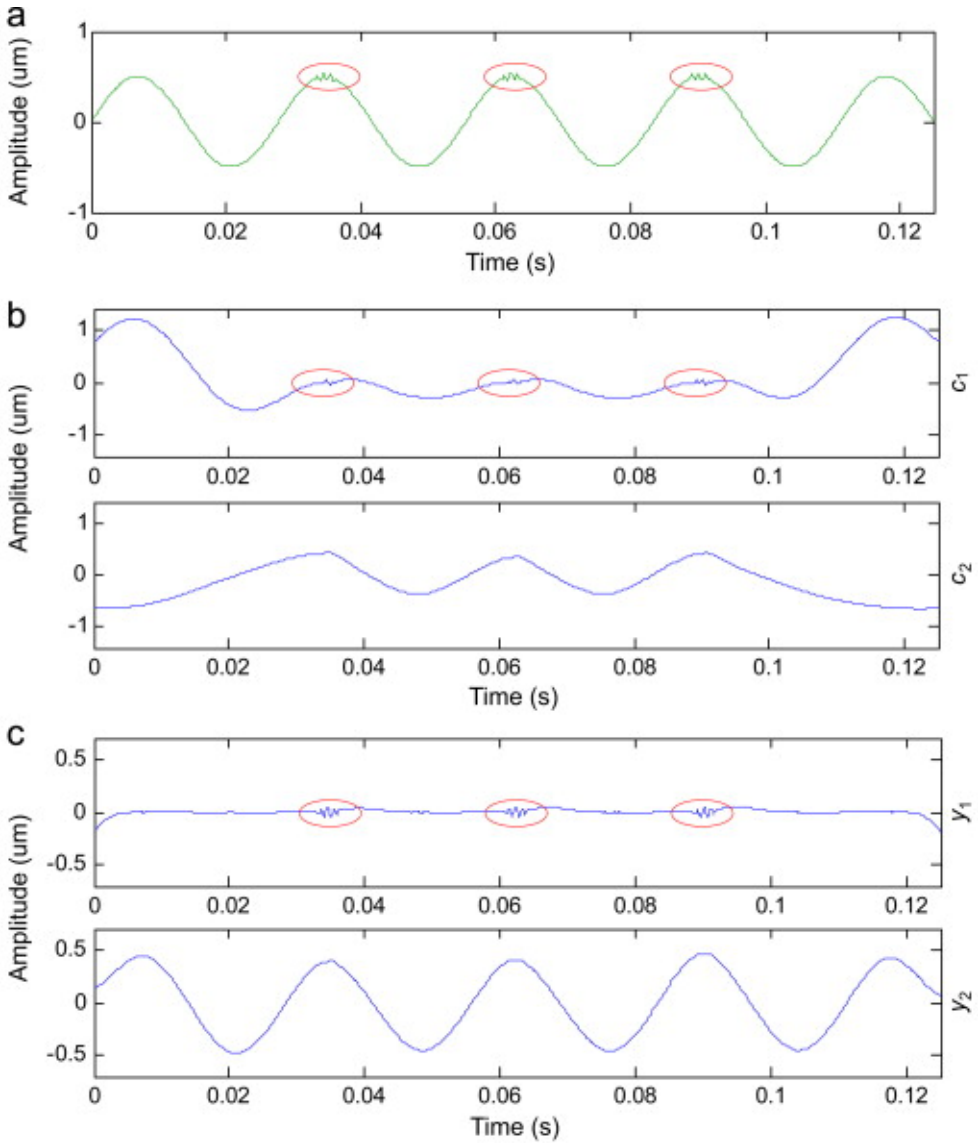

Figure 5.1: (a) A simulation signal, (b) IMFs c_1 and c_2 decomposed by EMD and (c) IMFs y_1 and y_2 decomposed by EEMD. Adapted from "A review on empirical mode decomposition in fault diagnosis of rotating machinery", by Y. Lei and J. Lin and Z. He and M. J. Zuo, 2013, Mechanical Systems and Signal Processing, 35 , p. 101–126. Copyright (2018) by Elsevier. Adapted with permission.

5.2 Pseudo EMD, Row-wise and Column-wise

In signal processing, EMD can be extended into a multiple-dimensional signal so that it can be applied to areas like image processing. Proposed by Chen et al. [6], pseudo-BEMD algorithm extends the 1D EMD to Bi-dimensional (BEMD) by translating the sifting process to each dimension and combine them together. For example, we have a 2D signal $X(i,j)$ of the size (i,j). First we perform EMD in one direction (like row-wise), apply the EMD on each row. Collecting the decomposed components of the same level m, we have m sets of 2D matrix, denoted as $RX(m,i,j)$. We have the following relationship

$$X(i,j) = \sum_{k=1}^{m} RX(k,i,j)\,. \tag{5.1}$$

The next step, naturally, is to decompose each column following the similar procedure as the previous step. This process will generate a 4D matrix $CRX(m,n,i,j)$, in which the m and n indices indicate the number of components from the row and then the column decomposition. We will then combine the components that of the same scale to generate 2D features with the best physical significance. The pseudo-BEMD method will then decompose the signal to be

$$C2D_L = \sum_{k=1}^{m} crx_{k,l} + \sum_{k=l+1}^{n} crx_{l,k}\,. \tag{5.2}$$

The last component is called the residue of the EMD. Although we only discusses the 2D case in this section, by following the similar process EMD can actually be extended to even higher dimensions.

5.3 Fast and Adaptive Bidimensional EMD

Fast and adaptive bidimensional EMD (FABEMD) was proposed in order to accelerate the EMD calculation [21], and now it has been applied in many areas like medical image analysis, texture analysis and so on. In the sifting process of EMD, calculating cubic spline requires solving a traditional matrix-vector equation. With a large number of iterations, it might take a long time to compute the IMFs. For 2D case BEMD will use surface interpolation, and it will cost even more computational resources. FABEMD is based on the algorithm of BEMD, but it modifies the interpolation step into a direct envelope estimation method and restricts the iterations to 1.

The details of the FABEMD method is discussed below: The first step of FABEMD is to detect the local maximum and minimum. Suppose we have a 2D matrix A_{ij} of the size $M \times N$. We can obtain the maximum and minimum value by sliding a window of size $\omega_{ex} \times \omega_{ex}$.

$$A = \begin{bmatrix} a_{11} & a_{12} & \dots & a_{1N} \\ a_{21} & a_{22} & \dots & a_{2N} \\ \vdots & \vdots & \dots & \vdots \\ a_{M1} & a_{M2} & \dots & a_{MN} \end{bmatrix}, \tag{5.3}$$

where a_{mn} is the element of A in the mth row and nth column. Let the window size be $\omega \times \omega$. Then the local maximum and local minimum will be extracted within the window for the given 2D data. After we obtain the maxima and minima maps, two order statistics, including MAX and MIN, will be used to approximating the upper and lower envelope. Order statistics filters are spatial filters whose response is based on the ordering of the elements contained within the data area encompassed by the filter. We then obtain the size of the window for the order-statistic filter. We define $d_{adj-max}$ and $d_{adj-min}$ to be the maximum and minimum distance in the array. Then we will build our square window, with the gross window width as the maximum of value of $maxd_{adj-max}, maxd_{adj-min}$ The next step is that, we will apply the MAX and MIN filter form to the 2D matrix to extract upper and lower envelopes using the parameters. With the determination of window size for envelope construction, MAX and MIN filters will then be applied to build upper and lower envelopes. To obtain smooth continuous surfaces, an averaging smoothing operation will be carried out on both envelopes. The rest of the procedure is similar to the classical BEMD algorithm. Simulation result of FABEMD shows that it can accelerate the computation by almost 10 times.

Chapter 6

2D Forward Diffusion Extension

In this chapter, we extend our new diffusion-based method to 2D, and show applications of the new method in image analysis.

6.1 Proposed Diffusion-based EMD Algorithms

As discussed briefly in Section 2, most EMD algorithms obtain the mean function from upper and lower envelopes which, in turn, are obtained by interpolating local maxima and minima of a function $S(x)$. All of these procedures are time-consuming and sensitive to error and noise.

In 2D case, our diffusion-based EMD method, on the other hand, is based on the the intuition that the "mean surface" of a signal can be constructed by the diffusion process. Instead of taking the average of two envelope surface functions of a signal $S(x)$ to produce a mean – Step 3 of the classical EMD algorithm in Section 2 – we directly diffuse the 2D signal to obtain the mean surface.

Recall that for the 1D case, we have to solve the following initial value problem (IVP) for the heat/diffusion equation,

$$\begin{aligned} \frac{\partial h}{\partial t} &= a\frac{\partial^2 h}{\partial x^2} \\ h(x,0) &= S(x)\,. \end{aligned} \tag{6.1}$$

For prescribed values of the diffusivity constant $a > 0$ (which can be adjusted) and time $T > 0$ we now define the *mean function* of $S(x)$ as $m(x) = h(x,T)$, i.e., the solution of

the IVP in Equation (4.5) at time T. In other words, the mean function $m(x)$ is obtained from $S(x)$ by a Gaussian filtering.

We extend the above PDE-based EMD method to the two-dimensional case by simply adding another spatial variable to the PDE in Equation (4.5), i.e.,

$$\begin{aligned} \frac{\partial h}{\partial t} &= a(\frac{\partial^2 h}{\partial x^2} + \frac{\partial^2 h}{\partial y^2}) \\ h(x, y, 0) &= S(x, y, 0)\,. \end{aligned} \tag{6.2}$$

The *mean function* of $S(x, y)$ will be defined as $m(x, y) = h(x, y, T)$.

In the 2D case, the motivations for this definition is that the time rate of change of $h(x, y, t)$ is zero at spatial inflection points of h. By connecting these spatial inflection points we can obtain the "mean surface". This is the basis of the following PDE-based BEMD algorithm applied to an image function $S(x, y)$:

1. Initialize: Let $n = 0$ and set $h_0(x, y, 0) = S(x, y)$.

2. Find the mean of $h_n(x, y, 0)$: Solve the PDE in Equation (6.2)) for $h_n(x, y, t)$ for $0 \leq t \leq T$. Then define $m_n(x, y) = h_n(x, y, T)$.

3. Extract mean: Define $c_n(x, y) = h_n(x, y, 0) - h_n(x, y, T)$.

4. If $c_n(x, y)$ is not a BIMF, let $h_{n+1}(x, y, 0) = c_n(x, y)$, $n \to n + 1$ and go to Step 2.

6.2 2D Mathematical Interpretation

As mentioned in Flandrin's paper [12, 13], traditional EMD operates as a successive filter when experimenting on Gaussian noise. In fact, we claim that traditional EMD operates as an iterative, frequency-overlapping, contrast-sensitive filter bank. This is also the case with our modified EMD and BEMD methods. In each iteration, the mean of the signal is obtained by passing it through a low-pass filter. Subsequent subtraction of the mean from the signal implies that the net procedure is equivalent to a high-pass filter. To illustrate, we consider the following special two-dimensional case,

$$S(x, y) = \sum_{i,j} [A_{ij} \sin(\omega_i x + \omega_j y + \phi_{ij})]\,, \tag{6.3}$$

where each (i, j) pair represents a single sinusoidal grating basis function. Equation (6.2)) is solved for the first mean function,

$$m_a(x, T) = \sum_{i,j} e^{-a\Omega_{ij}^2 T}[A_{ij} \sin(\omega_i x + \omega_j y + \phi_j)], \qquad \Omega_{ij} = \sqrt{\omega_i^2 + \omega_j^2}. \tag{6.4}$$

The magnitudes Ω_{ij} are now sorted in increasing order and denoted as Ω_k. We denote the sum of all components with the same Ω_k-value as s_k. After N iterations, our modified EMD algorithm yields the following result for $s_k(x)$,

$$\begin{aligned} h_{k,N} &= (1 - e^{-a\Omega_k^2 T})h_{k,N-1} \\ &= (1 - e^{-a\Omega_k^2 T})^N s_k \,. \end{aligned} \tag{6.5}$$

Now suppose, without loss of generality, that $\Omega_1 < \Omega_2 < \cdots < \Omega_K = \Omega_{\max}$. It is easy to show that for N sufficiently large,

$$\begin{aligned} h_N &= \sum_{k=1}^{K} (1 - e^{-a\Omega_k^2 T})^N s_k \\ &\simeq (1 - e^{-a\Omega_K^2 T})^N s_K \\ &\simeq s_K \,, \end{aligned} \tag{6.6}$$

where the final approximation is valid for T sufficiently large. By choosing the appropriate set of parameters, the IMF extracted after N iterations will be (at least approximately) the highest-frequency component, s_K. Our EMD algorithm, however, does not distinguish the direction of a frequency component (i.e., a particular sine grating) because the diffusion is *radial*. Instead, it will filter a group of frequency components Ω_{ij} that have the same "angular magnitude" Ω_k.

6.3 Experimental Results

We now show some results obtained by applying our diffusion-based EMD algorithm to some synthetic images [5], and some real images [15], A comparison of execution times between our method and classical BEMD is also presented.

6.3.1 PDE Implementation Scheme

Our current algorithm employs the simple explicit finite difference scheme for solving PDEs.

$$\frac{u_{i,j}^{n+1} - u_{i,j}^{n}}{\Delta t} = a(\frac{u_{i,j+1}^{n} - 2 * u_{i,j}^{n} + u_{i,j-1}^{n}}{\Delta x^2} + \frac{u_{i+1,j}^{n} - 2 * u_{i,j}^{n} + u_{i-1,j}^{n}}{\Delta y^2}) \,. \tag{6.7}$$

There are two options for boundary conditions (BCs): For an image whose edges are part of the background and of the same amplitude level, we have used Dirichlet BCs.

$$\begin{aligned} u(x_l, y_t, 0) &= s(x_l, y_t) \\ u(x_r, y_b, 0) &= s(x_l, y_t) \,, \end{aligned} \tag{6.8}$$

where x_l, x_r are the left and right end points, and y_t, y_b are the top and bottom end points, respectively. For an image with irregularly-shaped boundaries, we have used Neumann BCs.

$$\begin{aligned} u'(x_l, y_t, 0) &= 0 \\ u'(x_r, y_b, 0) &= 0 \,. \end{aligned} \tag{6.9}$$

The algorithm can also be implemented by convolution. Since we are solving a diffusion equation, it is possible to use a convolution to replace the finite difference / finite element approach (much faster). As for infinite long signal, the solution is equivalent to a convolution with a Gaussian function.

$$m_a(x) = \frac{1}{\sqrt{4\pi a t}} e^{-\frac{x^2}{4at}} * h_0(x, y) \,. \tag{6.10}$$

As discussed in section 4.4.1. Using zero-padded (corresponds to the Dirichlet BC.) or the replicate scheme (corresponds to the Neumann BC.) Gaussian function to convolve with the signal.

6.3.2 Simple Sine Gratings Image

In Figure 6.1, we display results for a 512×512-pixel synthetic image which consists of a mixture of two sine gratings. It has the form,

$$S(x, y) = \sin(0.1\pi x + 0.1\pi y) + \sin(-0.4\pi x + 0.8\pi y) \,. \tag{6.11}$$

The second (higher frequency) component is extracted as the first BIMF and the first component comprises the residual. The two sine gratings have been separated.

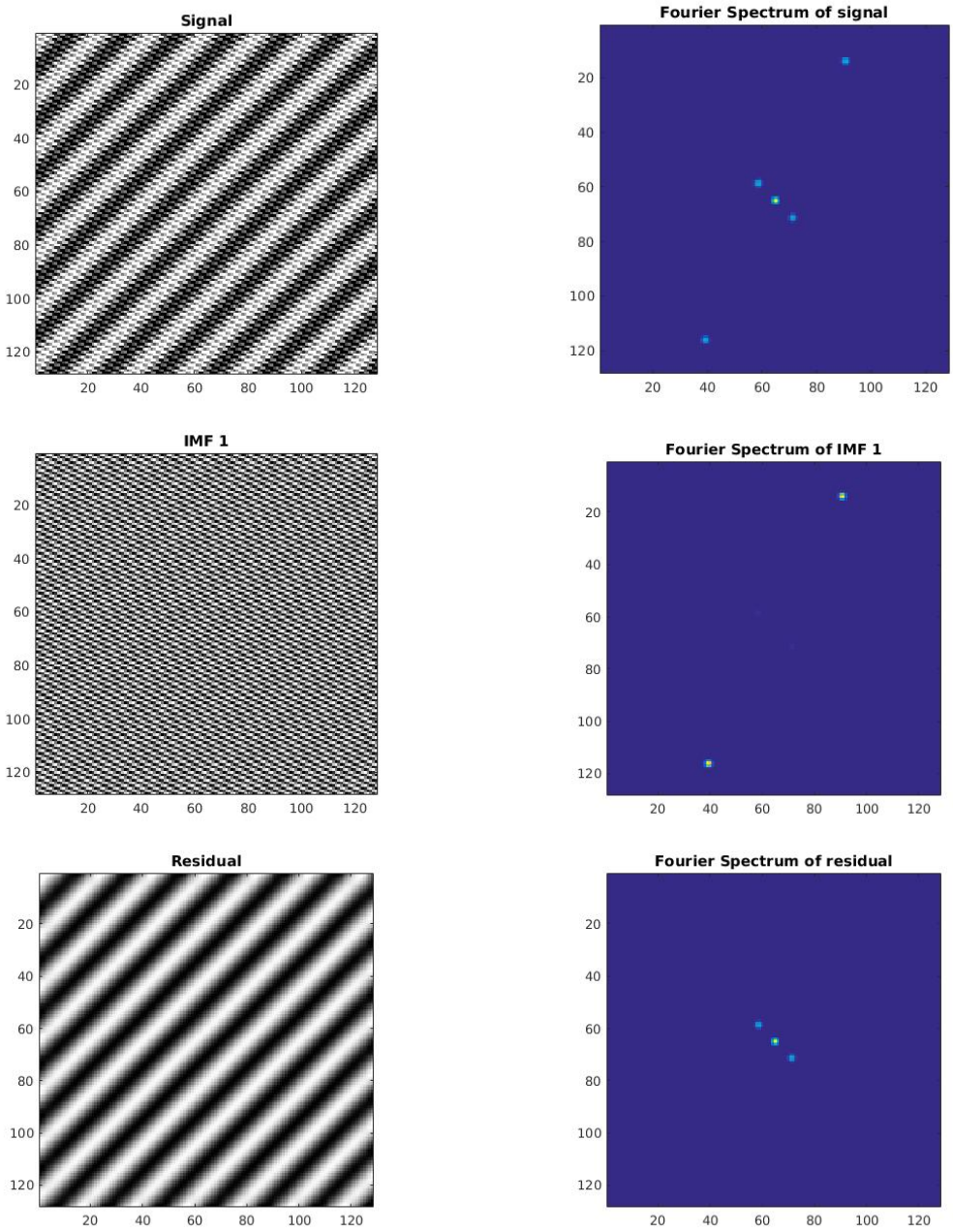

Figure 6.1: Simple sine gratings separation. **Top row:** Sine gratings mixture and its Fourier spectrum. **Middle row:** First BIMF and its Fourier spectrum. **Bottom row:** Residual and its Fourier spectrum.

6.3.3 Texture Image

In Figure 6.2 are shown the BIMF and residual when our diffusion-based BEMD algorithm is applied to a 512×512-pixel texture image selected from [5]. Successive BIMFs are comprised of lower frequency components of the texture.

6.3.4 Contrast-sensitive Image

The *contrast sensitivity function* (CSF) is an image which demonstrates the sensitivity of an observer to sine wave gratings of differing spatial frequencies [27]. Different frequency components are amplified to degrees which depend on their frequencies. The results obtained by applying our method to the CSF image are presented in Figure 6.3. Once again, the first BIMF contains the highest (horizontal) frequency components of the CSF which appears in the lower right of the image. The next BIMF contains slightly lower (horizontal) frequency components. Our method is seen to perform well in the separation of different (spatially-dependent) frequency components.

6.3.5 Blurred Mean Surface

In Figure 6.4 is shown the result of one application of the mean surface extraction method to the 512×512-pixel, 8 bits-per-pixel *Boat* image, using the parameter values $a = 4/\pi^2$ and $T = 50$.

6.3.6 Real Image

In Figure 6.5 are shown the results obtained by applying our algorithm to the 256×256-pixel, 8 bpp *Lena* image. Recalling that the sifting process of EMD/BEMD extracts IMFs with successively lower frequencies at each iteration, we note that the major contributions to the first two IMFs produced from the *Lena* image come, as expected, from its edges. Higher-order BIMFs contain lower-frequency features which are centered around the edges.

6.3.7 Comparison of Computational Costs

Traditional EMD and BEMD methods rely on finding local maxima and minima along with interpolation to find upper and lower envelope. This is computationally expensive,

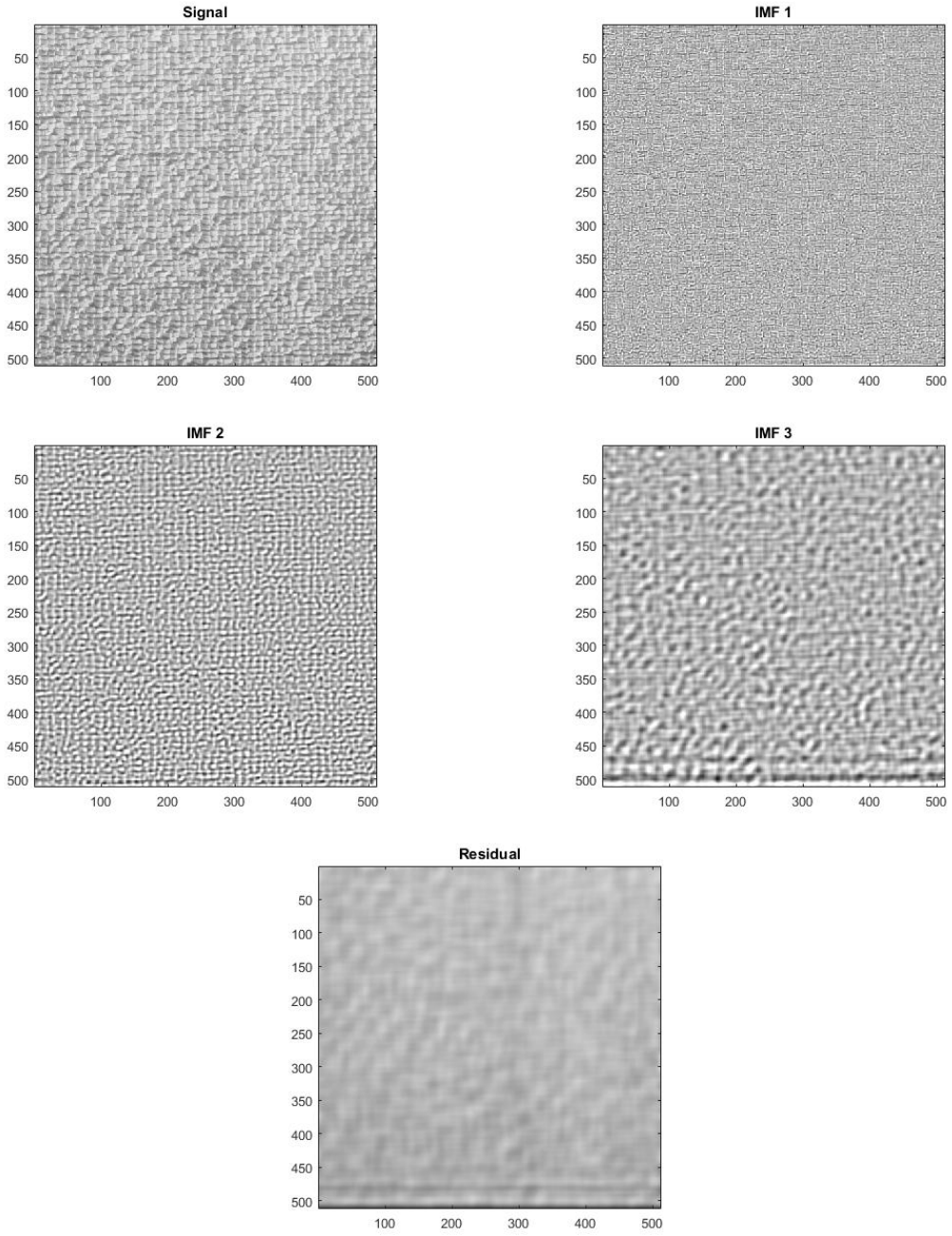

Figure 6.2: Example for texture decomposition. **Top two rows:** Raffia texture image from Brodatz [5] and its BIMFs. **Bottom row:** Residual.

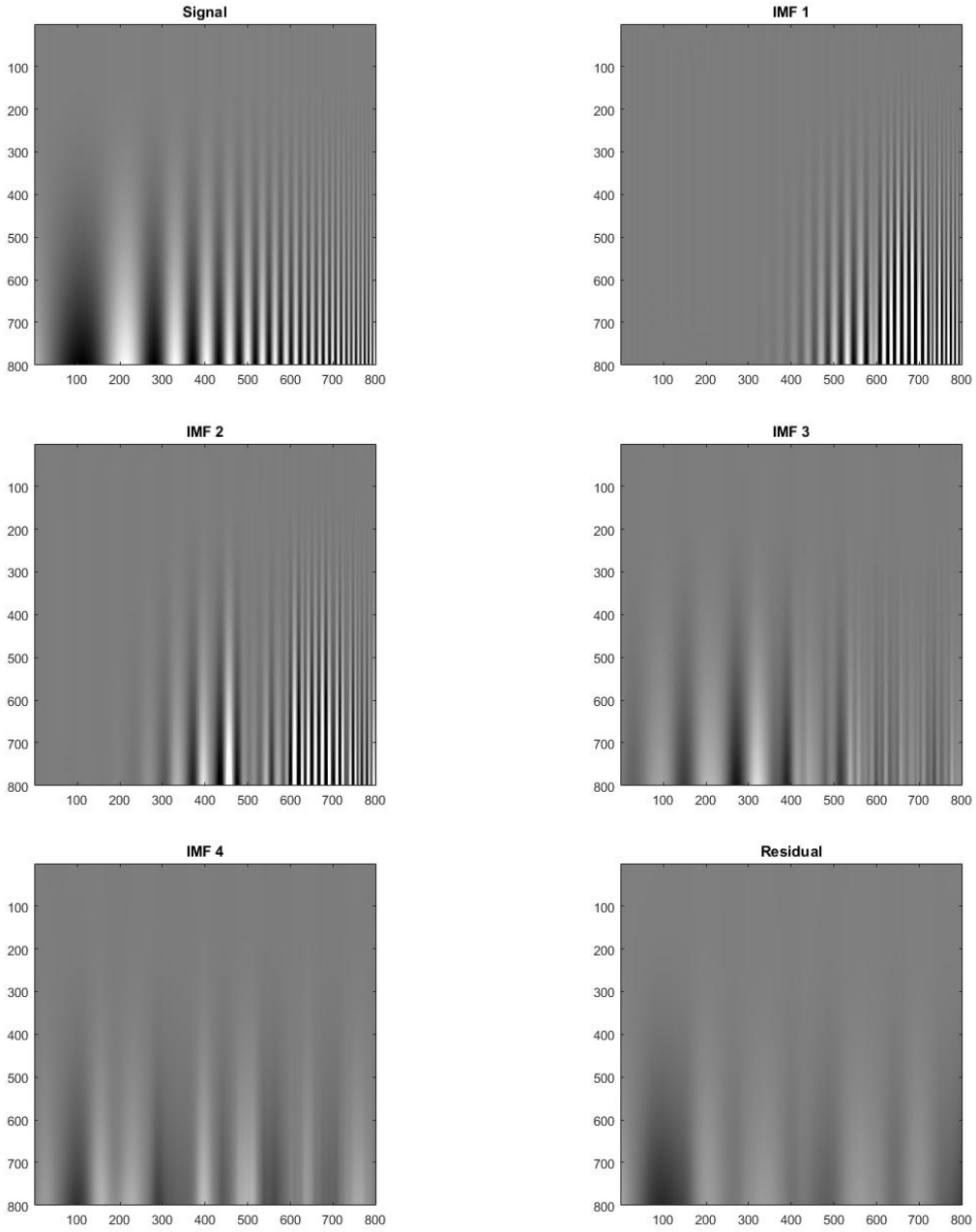

Figure 6.3: Contrast sensitive function (CSF) and corresponding BIMFs. **Top row:** CSF, first BIMF. **Middle row:** Second and third BIMFs. **Bottom row:** Fourth BIMF and residual.

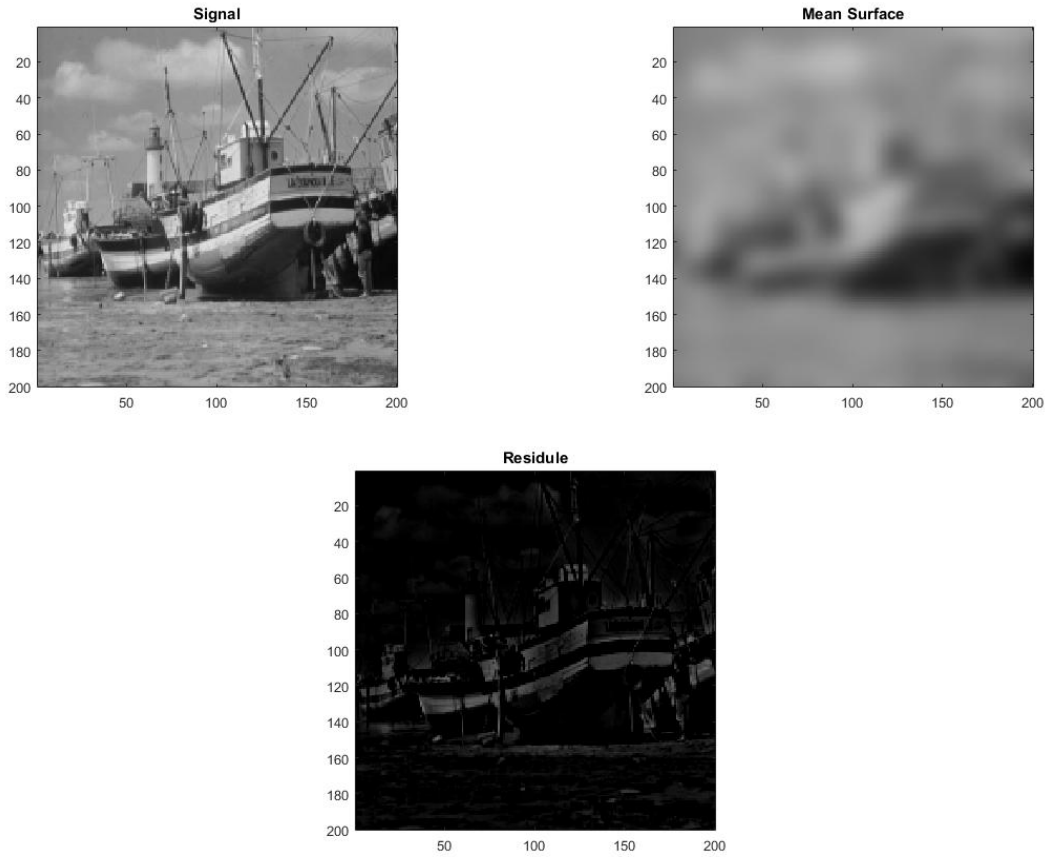

Figure 6.4: **Left:** Original *Boat* image. **Right:** Mean image $m_a(x, y)$. **Bottom:** Residual.

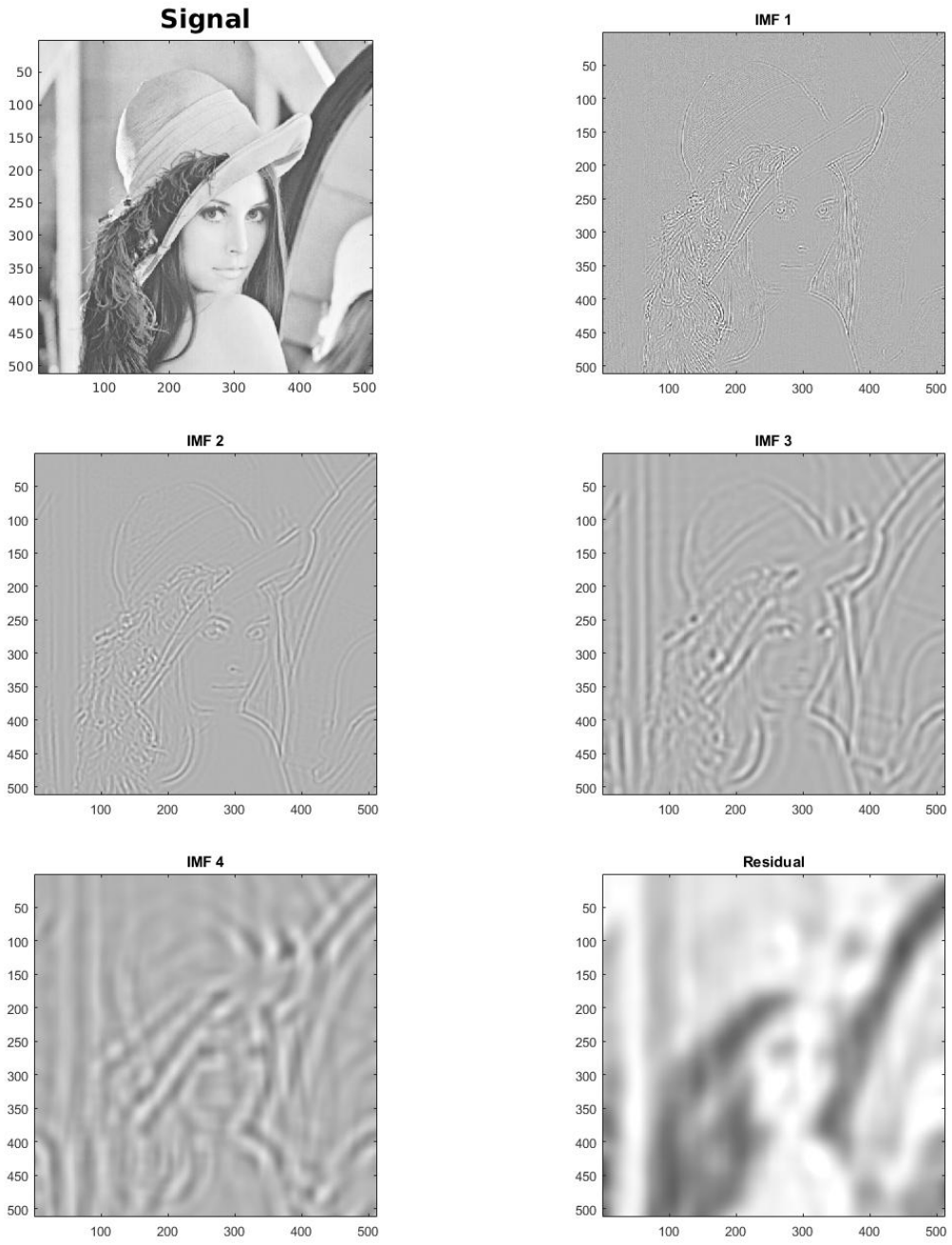

Figure 6.5: *Lena* image and its BIMFs. **Top row:** *Lena* image and the first BIMF. **Middle row:** Second and third BIMFs. **Bottom row:** fourth BIMF and the residual.

especially in the case of two dimensions, i.e., images. As such, our method could potentially require less computational time. To test this conjecture, we have determined the computational times required for a number of iterations of the sifting process for the classical BEMD method as well as our PDE-based BEMD method. (The code based on Flandrin's toolbox [24] was implemented for the classical BEMD method.) The results that obtained by experimenting on the *Lena* image, presented in the first two columns of Table 6.1, show that our diffusion-based method can decompose a given image into its BIMFs much faster than traditional BEMD.

	Trad. BEMD	**PDE-based EMD**	**PDE EMD with GC**
1 BIMF	4.18s	1.18s	0.13s
2 BIMFs	7.83s	2.24s	0.15s
3 BIMFs	11.16s	3.38s	0.27s
4 BIMFs	13.48s	4.48s	0.28s
5 BIMFs	15.29s	5.52s	0.49s

Table 6.1: Comparison of computational times for (i) traditional BEMD, (ii) diffusion-based BEMD and (iii) diffusion-based BEMD using Gaussian convolution (GC) in terms of total number of BIMFs computed

An even greater (on the order of tenfold) reduction in computational time is achieved if the finite difference computations involved in the determination of the mean surfaces $m_a(x, y)$ using Equation (6.2) are replaced by a single Gaussian convolution, as seen in the final column of Table 6.1. Technically, the solution of Equation (4.5) or Equation (6.2) is expressible as Gaussian convolution only in the case that the domain of definition is infinite, i.e., $\mathbb{R}$ or $\mathbb{R}^2$. By using convolution, we are essentially ignoring image boundary effects. In general, the differences between BIMFs obtained by finite differences and convolution are negligible except possibly near the image boundaries.

Chapter 7

Summary

In this thesis, we review the EMD signal analysis and discuss the advantages of our new proposed EMD modification. At the same time, we extend the discussion by describing some limitations of the current method and future potential.

7.1 Research Summary

EMD is a useful tool in signal processing, it decomposes signals into a subsequent sequences of frequency components. The major contribution of EMD is that it can extract the features adaptively, and is a pure data-driven method. The feature extraction steps of classic EMD unavoidably need the usage of interpolation, which increases the computational cost, as well as adding instabilities when processing noisy signals. Furthermore, a lack of a theoretical framework is the bottleneck of this analysis method. Engineers need to know the effective range of the application and why it fails for certain kinds of signals.

This thesis proposes a new diffusion-based EMD algorithm to tackle the problems mentioned above. The mean curve(surface) of a signal is obtained by evolving the signal with the heat/diffusion equation, therefore avoiding any complicated methods of extracting local maxima and minima and interpolating them. Our approach provides a mathematical interpretation of the EMD algorithm as well as its limitations. The parameters in the diffusion PDE can be adjusted according to the properties of the signal or image being analyzed. Our algorithm is considerably faster than traditional BEMD. Moreover, it is possible to accelerate the algorithm by using Gaussian convolution. A number of examples have shown that our method can extract multiscale features of images effectively. It has

been shown that, with a solid mathematical framework, our method can output similar separation performance compared with the traditional method. At the same time, robust to the mode-mixing signals (without noised assisted processing like EEMD). Finally, in experimentation, our method is 10-100 times faster when decomposing the same signals compared with EMD,

7.2 Further Exploration

Our method is adaptive and we have provided a way for parameter estimation. In order to extract the perfect features of a signal, however we need to have the prior knowledge. A possible solution is that we prefer a few trial experiments on the signals first, and then decide on the best parameter set or analysis method. Moreover, as shown in the separation performance section, the separation capability of the new method is limited just like the classic one. Even if we put huge computational resource, we cannot perfectly separate close frequency component. Realistic signals, most of the time, do not contain pure tones. Therefore EMD may output decomposition that does not fit the physical meaning of the original signals, and it might need further improvement on its robustness.

Letter of Copyright Permission

ELSEVIER LICENSE
TERMS AND CONDITIONS

Jun 20, 2018

This Agreement between 510 Blue Beech Blvd ("You") and Elsevier ("Elsevier") consists of your license details and the terms and conditions provided by Elsevier and Copyright Clearance Center.

License Number	4373261040754
License date	Jun 20, 2018
Licensed Content Publisher	Elsevier
Licensed Content Publication	Mechanical Systems and Signal Processing
Licensed Content Title	Elimination of end effects in empirical mode decomposition by mirror image coupled with support vector regression
Licensed Content Author	Da-Chao Lin,Zhang-Lin Guo,Feng-Ping An,Fan-Lei Zeng
Licensed Content Date	Aug 1, 2012
Licensed Content Volume	31
Licensed Content Issue	n/a
Licensed Content Pages	16
Start Page	13
End Page	28
Type of Use	reuse in a thesis/dissertation
Portion	figures/tables/illustrations
Number of figures/tables/illustrations	1
Format	both print and electronic
Are you the author of this Elsevier article?	No
Will you be translating?	No
Original figure numbers	Figure 1
Title of your thesis/dissertation	A Novel Diffusion-based Empirical Mode Decomposition Algorithm for Signal and Image Analysis
Expected completion date	Aug 2018
Estimated size (number of pages)	67
Requestor Location	510 Blue Beech Blvd 510 Blue Beech Blvd Waterloo, ON N2V2T3 Canada Attn: 510 Blue Beech Blvd
Publisher Tax ID	GB 494 6272 12
Total	0.00 CAD
Terms and Conditions	

INTRODUCTION

1. The publisher for this copyrighted material is Elsevier. By clicking "accept" in connection with completing this licensing transaction, you agree that the following terms and conditions apply to this transaction (along with the Billing and Payment terms and conditions established by Copyright Clearance Center, Inc. ("CCC"), at the time that you opened your Rightslink account and that are available at any time at http://myaccount.copyright.com).

GENERAL TERMS

2. Elsevier hereby grants you permission to reproduce the aforementioned material subject to the terms and conditions indicated.
3. Acknowledgement: If any part of the material to be used (for example, figures) has appeared in our publication with credit or acknowledgement to another source, permission must also be sought from that source. If such permission is not obtained then that material may not be included in your publication/copies. Suitable acknowledgement to the source must be made, either as a footnote or in a reference list at the end of your publication, as follows:
"Reprinted from Publication title, Vol /edition number, Author(s), Title of article / title of chapter, Pages No., Copyright (Year), with permission from Elsevier [OR APPLICABLE SOCIETY COPYRIGHT OWNER]." Also Lancet special credit - "Reprinted from The Lancet, Vol. number, Author(s), Title of article, Pages No., Copyright (Year), with permission from Elsevier."
4. Reproduction of this material is confined to the purpose and/or media for which permission is hereby given.
5. Altering/Modifying Material: Not Permitted. However figures and illustrations may be altered/adapted minimally to serve your work. Any other abbreviations, additions, deletions and/or any other alterations shall be made only with prior written authorization of Elsevier Ltd. (Please contact Elsevier at permissions@elsevier.com). No modifications can be made to any Lancet figures/tables and they must be reproduced in full.
6. If the permission fee for the requested use of our material is waived in this instance, please be advised that your future requests for Elsevier materials may attract a fee.
7. Reservation of Rights: Publisher reserves all rights not specifically granted in the combination of (i) the license details provided by you and accepted in the course of this licensing transaction, (ii) these terms and conditions and (iii) CCC's Billing and Payment terms and conditions.
8. License Contingent Upon Payment: While you may exercise the rights licensed immediately upon issuance of the license at the end of the licensing process for the transaction, provided that you have disclosed complete and accurate details of your proposed use, no license is finally effective unless and until full payment is received from you (either by publisher or by CCC) as provided in CCC's Billing and Payment terms and conditions. If full payment is not received on a timely basis, then any license preliminarily granted shall be deemed automatically revoked and shall be void as if never granted. Further, in the event that you breach any of these terms and conditions or any of CCC's Billing and Payment terms and conditions, the license is automatically revoked and shall be void as if never granted. Use of materials as described in a revoked license, as well as any use of the materials beyond the scope of an unrevoked license, may constitute copyright infringement and publisher reserves the right to take any and all action to protect its copyright in the materials.
9. Warranties: Publisher makes no representations or warranties with respect to the licensed material.
10. Indemnity: You hereby indemnify and agree to hold harmless publisher and CCC, and their respective officers, directors, employees and agents, from and against any and all claims arising out of your use of the licensed material other than as specifically authorized pursuant to this license.
11. No Transfer of License: This license is personal to you and may not be sublicensed, assigned, or transferred by you to any other person without publisher's written permission.

12. No Amendment Except in Writing: This license may not be amended except in a writing signed by both parties (or, in the case of publisher, by CCC on publisher's behalf).
13. Objection to Contrary Terms: Publisher hereby objects to any terms contained in any purchase order, acknowledgment, check endorsement or other writing prepared by you, which terms are inconsistent with these terms and conditions or CCC's Billing and Payment terms and conditions. These terms and conditions, together with CCC's Billing and Payment terms and conditions (which are incorporated herein), comprise the entire agreement between you and publisher (and CCC) concerning this licensing transaction. In the event of any conflict between your obligations established by these terms and conditions and those established by CCC's Billing and Payment terms and conditions, these terms and conditions shall control.
14. Revocation: Elsevier or Copyright Clearance Center may deny the permissions described in this License at their sole discretion, for any reason or no reason, with a full refund payable to you. Notice of such denial will be made using the contact information provided by you. Failure to receive such notice will not alter or invalidate the denial. In no event will Elsevier or Copyright Clearance Center be responsible or liable for any costs, expenses or damage incurred by you as a result of a denial of your permission request, other than a refund of the amount(s) paid by you to Elsevier and/or Copyright Clearance Center for denied permissions.

LIMITED LICENSE

The following terms and conditions apply only to specific license types:
15. **Translation**: This permission is granted for non-exclusive world **English** rights only unless your license was granted for translation rights. If you licensed translation rights you may only translate this content into the languages you requested. A professional translator must perform all translations and reproduce the content word for word preserving the integrity of the article.
16. **Posting licensed content on any Website**: The following terms and conditions apply as follows: Licensing material from an Elsevier journal: All content posted to the web site must maintain the copyright information line on the bottom of each image; A hyper-text must be included to the Homepage of the journal from which you are licensing at http://www.sciencedirect.com/science/journal/xxxxx or the Elsevier homepage for books at http://www.elsevier.com; Central Storage: This license does not include permission for a scanned version of the material to be stored in a central repository such as that provided by Heron/XanEdu.
Licensing material from an Elsevier book: A hyper-text link must be included to the Elsevier homepage at http://www.elsevier.com . All content posted to the web site must maintain the copyright information line on the bottom of each image.

Posting licensed content on Electronic reserve: In addition to the above the following clauses are applicable: The web site must be password-protected and made available only to bona fide students registered on a relevant course. This permission is granted for 1 year only. You may obtain a new license for future website posting.
17. **For journal authors:** the following clauses are applicable in addition to the above:
Preprints:
A preprint is an author's own write-up of research results and analysis, it has not been peer-reviewed, nor has it had any other value added to it by a publisher (such as formatting, copyright, technical enhancement etc.).
Authors can share their preprints anywhere at any time. Preprints should not be added to or enhanced in any way in order to appear more like, or to substitute for, the final versions of articles however authors can update their preprints on arXiv or RePEc with their Accepted Author Manuscript (see below).
If accepted for publication, we encourage authors to link from the preprint to their formal publication via its DOI. Millions of researchers have access to the formal publications on ScienceDirect, and so links will help users to find, access, cite and use the best available

version. Please note that Cell Press, The Lancet and some society-owned have different preprint policies. Information on these policies is available on the journal homepage.
Accepted Author Manuscripts: An accepted author manuscript is the manuscript of an article that has been accepted for publication and which typically includes author-incorporated changes suggested during submission, peer review and editor-author communications.
Authors can share their accepted author manuscript:

- immediately
  - via their non-commercial person homepage or blog
  - by updating a preprint in arXiv or RePEc with the accepted manuscript
  - via their research institute or institutional repository for internal institutional uses or as part of an invitation-only research collaboration work-group
  - directly by providing copies to their students or to research collaborators for their personal use
  - for private scholarly sharing as part of an invitation-only work group on commercial sites with which Elsevier has an agreement
- After the embargo period
  - via non-commercial hosting platforms such as their institutional repository
  - via commercial sites with which Elsevier has an agreement

In all cases accepted manuscripts should:

- link to the formal publication via its DOI
- bear a CC-BY-NC-ND license - this is easy to do
- if aggregated with other manuscripts, for example in a repository or other site, be shared in alignment with our hosting policy not be added to or enhanced in any way to appear more like, or to substitute for, the published journal article.

Published journal article (JPA): A published journal article (PJA) is the definitive final record of published research that appears or will appear in the journal and embodies all value-adding publishing activities including peer review co-ordination, copy-editing, formatting, (if relevant) pagination and online enrichment.
Policies for sharing publishing journal articles differ for subscription and gold open access articles:
Subscription Articles: If you are an author, please share a link to your article rather than the full-text. Millions of researchers have access to the formal publications on ScienceDirect, and so links will help your users to find, access, cite, and use the best available version.
Theses and dissertations which contain embedded PJAs as part of the formal submission can be posted publicly by the awarding institution with DOI links back to the formal publications on ScienceDirect.
If you are affiliated with a library that subscribes to ScienceDirect you have additional private sharing rights for others' research accessed under that agreement. This includes use for classroom teaching and internal training at the institution (including use in course packs and courseware programs), and inclusion of the article for grant funding purposes.
Gold Open Access Articles: May be shared according to the author-selected end-user license and should contain a CrossMark logo, the end user license, and a DOI link to the formal publication on ScienceDirect.
Please refer to Elsevier's posting policy for further information.
18. **For book authors** the following clauses are applicable in addition to the above:
Authors are permitted to place a brief summary of their work online only. You are not allowed to download and post the published electronic version of your chapter, nor may you scan the printed edition to create an electronic version. **Posting to a repository:** Authors are permitted to post a summary of their chapter only in their institution's repository.

19. **Thesis/Dissertation**: If your license is for use in a thesis/dissertation your thesis may be submitted to your institution in either print or electronic form. Should your thesis be published commercially, please reapply for permission. These requirements include permission for the Library and Archives of Canada to supply single copies, on demand, of the complete thesis and include permission for Proquest/UMI to supply single copies, on demand, of the complete thesis. Should your thesis be published commercially, please reapply for permission. Theses and dissertations which contain embedded PJAs as part of the formal submission can be posted publicly by the awarding institution with DOI links back to the formal publications on ScienceDirect.

Elsevier Open Access Terms and Conditions

You can publish open access with Elsevier in hundreds of open access journals or in nearly 2000 established subscription journals that support open access publishing. Permitted third party re-use of these open access articles is defined by the author's choice of Creative Commons user license. See our open access license policy for more information.

Terms & Conditions applicable to all Open Access articles published with Elsevier:

Any reuse of the article must not represent the author as endorsing the adaptation of the article nor should the article be modified in such a way as to damage the author's honour or reputation. If any changes have been made, such changes must be clearly indicated.

The author(s) must be appropriately credited and we ask that you include the end user license and a DOI link to the formal publication on ScienceDirect.

If any part of the material to be used (for example, figures) has appeared in our publication with credit or acknowledgement to another source it is the responsibility of the user to ensure their reuse complies with the terms and conditions determined by the rights holder.

Additional Terms & Conditions applicable to each Creative Commons user license:

CC BY: The CC-BY license allows users to copy, to create extracts, abstracts and new works from the Article, to alter and revise the Article and to make commercial use of the Article (including reuse and/or resale of the Article by commercial entities), provided the user gives appropriate credit (with a link to the formal publication through the relevant DOI), provides a link to the license, indicates if changes were made and the licensor is not represented as endorsing the use made of the work. The full details of the license are available at http://creativecommons.org/licenses/by/4.0.

CC BY NC SA: The CC BY-NC-SA license allows users to copy, to create extracts, abstracts and new works from the Article, to alter and revise the Article, provided this is not done for commercial purposes, and that the user gives appropriate credit (with a link to the formal publication through the relevant DOI), provides a link to the license, indicates if changes were made and the licensor is not represented as endorsing the use made of the work. Further, any new works must be made available on the same conditions. The full details of the license are available at http://creativecommons.org/licenses/by-nc-sa/4.0.

CC BY NC ND: The CC BY-NC-ND license allows users to copy and distribute the Article, provided this is not done for commercial purposes and further does not permit distribution of the Article if it is changed or edited in any way, and provided the user gives appropriate credit (with a link to the formal publication through the relevant DOI), provides a link to the license, and that the licensor is not represented as endorsing the use made of the work. The full details of the license are available at http://creativecommons.org/licenses/by-nc-nd/4.0.

Any commercial reuse of Open Access articles published with a CC BY NC SA or CC BY NC ND license requires permission from Elsevier and will be subject to a fee.

Commercial reuse includes:

- Associating advertising with the full text of the Article
- Charging fees for document delivery or access
- Article aggregation
- Systematic distribution via e-mail lists or share buttons

Posting or linking by commercial companies for use by customers of those companies.

20. **Other Conditions**:

v1.9

ELSEVIER LICENSE
TERMS AND CONDITIONS

Jun 20, 2018

This Agreement between 510 Blue Beech Blvd ("You") and Elsevier ("Elsevier") consists of your license details and the terms and conditions provided by Elsevier and Copyright Clearance Center.

License Number	4373351294757
License date	Jun 20, 2018
Licensed Content Publisher	Elsevier
Licensed Content Publication	Mechanical Systems and Signal Processing
Licensed Content Title	A review on empirical mode decomposition in fault diagnosis of rotating machinery
Licensed Content Author	Yaguo Lei,Jing Lin,Zhengjia He,Ming J. Zuo
Licensed Content Date	Feb 1, 2013
Licensed Content Volume	35
Licensed Content Issue	1-2
Licensed Content Pages	19
Start Page	108
End Page	126
Type of Use	reuse in a thesis/dissertation
Intended publisher of new work	other
Portion	figures/tables/illustrations
Number of figures/tables/illustrations	5
Format	both print and electronic
Are you the author of this Elsevier article?	No
Will you be translating?	No
Original figure numbers	Figure.5
Title of your thesis/dissertation	A Novel Diffusion-based Empirical Mode Decomposition Algorithm for Signal and Image Analysis
Expected completion date	Aug 2018
Estimated size (number of pages)	67
Requestor Location	510 Blue Beech Blvd 510 Blue Beech Blvd Waterloo, ON N2V2T3 Canada Attn: 510 Blue Beech Blvd
Publisher Tax ID	GB 494 6272 12
Total	0.00 CAD
Terms and Conditions	

INTRODUCTION

1. The publisher for this copyrighted material is Elsevier. By clicking "accept" in connection with completing this licensing transaction, you agree that the following terms and conditions apply to this transaction (along with the Billing and Payment terms and conditions established by Copyright Clearance Center, Inc. ("CCC"), at the time that you opened your Rightslink account and that are available at any time at http://myaccount.copyright.com).

GENERAL TERMS

2. Elsevier hereby grants you permission to reproduce the aforementioned material subject to the terms and conditions indicated.
3. Acknowledgement: If any part of the material to be used (for example, figures) has appeared in our publication with credit or acknowledgement to another source, permission must also be sought from that source. If such permission is not obtained then that material may not be included in your publication/copies. Suitable acknowledgement to the source must be made, either as a footnote or in a reference list at the end of your publication, as follows:
"Reprinted from Publication title, Vol /edition number, Author(s), Title of article / title of chapter, Pages No., Copyright (Year), with permission from Elsevier [OR APPLICABLE SOCIETY COPYRIGHT OWNER]." Also Lancet special credit - "Reprinted from The Lancet, Vol. number, Author(s), Title of article, Pages No., Copyright (Year), with permission from Elsevier."
4. Reproduction of this material is confined to the purpose and/or media for which permission is hereby given.
5. Altering/Modifying Material: Not Permitted. However figures and illustrations may be altered/adapted minimally to serve your work. Any other abbreviations, additions, deletions and/or any other alterations shall be made only with prior written authorization of Elsevier Ltd. (Please contact Elsevier at permissions@elsevier.com). No modifications can be made to any Lancet figures/tables and they must be reproduced in full.
6. If the permission fee for the requested use of our material is waived in this instance, please be advised that your future requests for Elsevier materials may attract a fee.
7. Reservation of Rights: Publisher reserves all rights not specifically granted in the combination of (i) the license details provided by you and accepted in the course of this licensing transaction, (ii) these terms and conditions and (iii) CCC's Billing and Payment terms and conditions.
8. License Contingent Upon Payment: While you may exercise the rights licensed immediately upon issuance of the license at the end of the licensing process for the transaction, provided that you have disclosed complete and accurate details of your proposed use, no license is finally effective unless and until full payment is received from you (either by publisher or by CCC) as provided in CCC's Billing and Payment terms and conditions. If full payment is not received on a timely basis, then any license preliminarily granted shall be deemed automatically revoked and shall be void as if never granted. Further, in the event that you breach any of these terms and conditions or any of CCC's Billing and Payment terms and conditions, the license is automatically revoked and shall be void as if never granted. Use of materials as described in a revoked license, as well as any use of the materials beyond the scope of an unrevoked license, may constitute copyright infringement and publisher reserves the right to take any and all action to protect its copyright in the materials.
9. Warranties: Publisher makes no representations or warranties with respect to the licensed material.
10. Indemnity: You hereby indemnify and agree to hold harmless publisher and CCC, and their respective officers, directors, employees and agents, from and against any and all claims arising out of your use of the licensed material other than as specifically authorized pursuant to this license.
11. No Transfer of License: This license is personal to you and may not be sublicensed, assigned, or transferred by you to any other person without publisher's written permission.

12. No Amendment Except in Writing: This license may not be amended except in a writing signed by both parties (or, in the case of publisher, by CCC on publisher's behalf).
13. Objection to Contrary Terms: Publisher hereby objects to any terms contained in any purchase order, acknowledgment, check endorsement or other writing prepared by you, which terms are inconsistent with these terms and conditions or CCC's Billing and Payment terms and conditions. These terms and conditions, together with CCC's Billing and Payment terms and conditions (which are incorporated herein), comprise the entire agreement between you and publisher (and CCC) concerning this licensing transaction. In the event of any conflict between your obligations established by these terms and conditions and those established by CCC's Billing and Payment terms and conditions, these terms and conditions shall control.
14. Revocation: Elsevier or Copyright Clearance Center may deny the permissions described in this License at their sole discretion, for any reason or no reason, with a full refund payable to you. Notice of such denial will be made using the contact information provided by you. Failure to receive such notice will not alter or invalidate the denial. In no event will Elsevier or Copyright Clearance Center be responsible or liable for any costs, expenses or damage incurred by you as a result of a denial of your permission request, other than a refund of the amount(s) paid by you to Elsevier and/or Copyright Clearance Center for denied permissions.

LIMITED LICENSE

The following terms and conditions apply only to specific license types:
15. **Translation**: This permission is granted for non-exclusive world **English** rights only unless your license was granted for translation rights. If you licensed translation rights you may only translate this content into the languages you requested. A professional translator must perform all translations and reproduce the content word for word preserving the integrity of the article.
16. **Posting licensed content on any Website**: The following terms and conditions apply as follows: Licensing material from an Elsevier journal: All content posted to the web site must maintain the copyright information line on the bottom of each image; A hyper-text must be included to the Homepage of the journal from which you are licensing at http://www.sciencedirect.com/science/journal/xxxxx or the Elsevier homepage for books at http://www.elsevier.com; Central Storage: This license does not include permission for a scanned version of the material to be stored in a central repository such as that provided by Heron/XanEdu.
Licensing material from an Elsevier book: A hyper-text link must be included to the Elsevier homepage at http://www.elsevier.com . All content posted to the web site must maintain the copyright information line on the bottom of each image.

Posting licensed content on Electronic reserve: In addition to the above the following clauses are applicable: The web site must be password-protected and made available only to bona fide students registered on a relevant course. This permission is granted for 1 year only. You may obtain a new license for future website posting.
17. **For journal authors:** the following clauses are applicable in addition to the above:
Preprints:
A preprint is an author's own write-up of research results and analysis, it has not been peer-reviewed, nor has it had any other value added to it by a publisher (such as formatting, copyright, technical enhancement etc.).
Authors can share their preprints anywhere at any time. Preprints should not be added to or enhanced in any way in order to appear more like, or to substitute for, the final versions of articles however authors can update their preprints on arXiv or RePEc with their Accepted Author Manuscript (see below).
If accepted for publication, we encourage authors to link from the preprint to their formal publication via its DOI. Millions of researchers have access to the formal publications on ScienceDirect, and so links will help users to find, access, cite and use the best available

version. Please note that Cell Press, The Lancet and some society-owned have different preprint policies. Information on these policies is available on the journal homepage.
Accepted Author Manuscripts: An accepted author manuscript is the manuscript of an article that has been accepted for publication and which typically includes author-incorporated changes suggested during submission, peer review and editor-author communications.
Authors can share their accepted author manuscript:

- immediately
  - via their non-commercial person homepage or blog
  - by updating a preprint in arXiv or RePEc with the accepted manuscript
  - via their research institute or institutional repository for internal institutional uses or as part of an invitation-only research collaboration work-group
  - directly by providing copies to their students or to research collaborators for their personal use
  - for private scholarly sharing as part of an invitation-only work group on commercial sites with which Elsevier has an agreement
- After the embargo period
  - via non-commercial hosting platforms such as their institutional repository
  - via commercial sites with which Elsevier has an agreement

In all cases accepted manuscripts should:

- link to the formal publication via its DOI
- bear a CC-BY-NC-ND license - this is easy to do
- if aggregated with other manuscripts, for example in a repository or other site, be shared in alignment with our hosting policy not be added to or enhanced in any way to appear more like, or to substitute for, the published journal article.

Published journal article (JPA): A published journal article (PJA) is the definitive final record of published research that appears or will appear in the journal and embodies all value-adding publishing activities including peer review co-ordination, copy-editing, formatting, (if relevant) pagination and online enrichment.
Policies for sharing publishing journal articles differ for subscription and gold open access articles:
Subscription Articles: If you are an author, please share a link to your article rather than the full-text. Millions of researchers have access to the formal publications on ScienceDirect, and so links will help your users to find, access, cite, and use the best available version.
Theses and dissertations which contain embedded PJAs as part of the formal submission can be posted publicly by the awarding institution with DOI links back to the formal publications on ScienceDirect.
If you are affiliated with a library that subscribes to ScienceDirect you have additional private sharing rights for others' research accessed under that agreement. This includes use for classroom teaching and internal training at the institution (including use in course packs and courseware programs), and inclusion of the article for grant funding purposes.
Gold Open Access Articles: May be shared according to the author-selected end-user license and should contain a CrossMark logo, the end user license, and a DOI link to the formal publication on ScienceDirect.
Please refer to Elsevier's posting policy for further information.
18. **For book authors** the following clauses are applicable in addition to the above:
Authors are permitted to place a brief summary of their work online only. You are not allowed to download and post the published electronic version of your chapter, nor may you scan the printed edition to create an electronic version. **Posting to a repository:** Authors are permitted to post a summary of their chapter only in their institution's repository.

19. **Thesis/Dissertation**: If your license is for use in a thesis/dissertation your thesis may be submitted to your institution in either print or electronic form. Should your thesis be published commercially, please reapply for permission. These requirements include permission for the Library and Archives of Canada to supply single copies, on demand, of the complete thesis and include permission for Proquest/UMI to supply single copies, on demand, of the complete thesis. Should your thesis be published commercially, please reapply for permission. Theses and dissertations which contain embedded PJAs as part of the formal submission can be posted publicly by the awarding institution with DOI links back to the formal publications on ScienceDirect.

Elsevier Open Access Terms and Conditions

You can publish open access with Elsevier in hundreds of open access journals or in nearly 2000 established subscription journals that support open access publishing. Permitted third party re-use of these open access articles is defined by the author's choice of Creative Commons user license. See our open access license policy for more information.

Terms & Conditions applicable to all Open Access articles published with Elsevier:

Any reuse of the article must not represent the author as endorsing the adaptation of the article nor should the article be modified in such a way as to damage the author's honour or reputation. If any changes have been made, such changes must be clearly indicated.

The author(s) must be appropriately credited and we ask that you include the end user license and a DOI link to the formal publication on ScienceDirect.

If any part of the material to be used (for example, figures) has appeared in our publication with credit or acknowledgement to another source it is the responsibility of the user to ensure their reuse complies with the terms and conditions determined by the rights holder.

Additional Terms & Conditions applicable to each Creative Commons user license:

CC BY: The CC-BY license allows users to copy, to create extracts, abstracts and new works from the Article, to alter and revise the Article and to make commercial use of the Article (including reuse and/or resale of the Article by commercial entities), provided the user gives appropriate credit (with a link to the formal publication through the relevant DOI), provides a link to the license, indicates if changes were made and the licensor is not represented as endorsing the use made of the work. The full details of the license are available at http://creativecommons.org/licenses/by/4.0.

CC BY NC SA: The CC BY-NC-SA license allows users to copy, to create extracts, abstracts and new works from the Article, to alter and revise the Article, provided this is not done for commercial purposes, and that the user gives appropriate credit (with a link to the formal publication through the relevant DOI), provides a link to the license, indicates if changes were made and the licensor is not represented as endorsing the use made of the work. Further, any new works must be made available on the same conditions. The full details of the license are available at http://creativecommons.org/licenses/by-nc-sa/4.0.

CC BY NC ND: The CC BY-NC-ND license allows users to copy and distribute the Article, provided this is not done for commercial purposes and further does not permit distribution of the Article if it is changed or edited in any way, and provided the user gives appropriate credit (with a link to the formal publication through the relevant DOI), provides a link to the license, and that the licensor is not represented as endorsing the use made of the work. The full details of the license are available at http://creativecommons.org/licenses/by-nc-nd/4.0.

Any commercial reuse of Open Access articles published with a CC BY NC SA or CC BY NC ND license requires permission from Elsevier and will be subject to a fee.

Commercial reuse includes:

- Associating advertising with the full text of the Article
- Charging fees for document delivery or access
- Article aggregation
- Systematic distribution via e-mail lists or share buttons

Posting or linking by commercial companies for use by customers of those companies.

20. **Other Conditions**:

v1.9

References

[1] J. Allen. Short term spectral analysis, synthesis, and modification by discrete fourier transform. *IEEE Transactions on Acoustics, Speech, and Signal Processing*, 25(3):235–238, 1977.

[2] V. Bajaj and R. B. Pachori. Classification of seizure and nonseizure eeg signals using empirical mode decomposition. *IEEE Transactions on Information Technology in Biomedicine*, 16(6):1135–1142, 2012.

[3] J. S. Bendat and A. G. Piersol. *Random data: analysis and measurement procedures*, volume 729. John Wiley & Sons, 2011.

[4] E. Brevdo, N. S. Fučkar, G. Thakur, and H. T. Wu. The synchrosqueezing algorithm: a robust analysis tool for signals with time-varying spectrum. Technical report, 2011.

[5] P. Brodatz. *Textures: a photographic album for artists and designers*. Dover Pubns, 1966.

[6] C. Y. Chen, S. M. Guo, W. S. Chang, J. S. H. Tsai, and K. S. Cheng. An improved bidimensional empirical mode decomposition: A mean approach for fast decomposition. *Signal Processing*, 98:344–358, 2014.

[7] I. Daubechies. Orthonormal bases of compactly supported wavelets. *Communications on pure and applied mathematics*, 41(7):909–996, 1988.

[8] I. Daubechies, J. Lu, and H. T. Wu. Synchrosqueezed wavelet transforms: An empirical mode decomposition-like tool. *Applied and computational harmonic analysis*, 30(2):243–261, 2011.

[9] E. Deléchelle, J. Lemoine, and O. Niang. Empirical mode decomposition: An analytical approach for sifting process. *IEEE Signal Processing Letters*, 12(11):764–767, 2005.

[10] H. El, S. Diop, R. Alexandre, and A. O. Boudraa. A pde characterization of the intrinsic mode functions. In *Acoustics, Speech and Signal Processing, 2009. ICASSP 2009. IEEE International Conference on*, pages 3429–3432. IEEE, 2009.

[11] H. El, S. Diop, R. Alexandre, and A. O. Boudraa. Analysis of intrinsic mode functions: a pde approach. *IEEE Signal Processing Letters*, 17(4):398–401, 2010.

[12] P. Flandrin, P. Gonçalves, and G. Rilling. Emd equivalent filter banks, from interpretation to applications. In *Hilbert–Huang transform and its applications*, pages 99–116. World Scientific, 2014.

[13] P. Flandrin, G. Rilling, and P. Goncalves. Empirical mode decomposition as a filter bank. *IEEE signal processing letters*, 11(2):112–114, 2004.

[14] A. L. Goldberger, L. A. Amaral, L. Glass, J. M. Hausdorff, P. C. Ivanov, R. G. Mark, J. E. Mietus, E. Joseph, G. B. Moody, C. K. Peng, and H. E. Stanley. Physiobank, physiotoolkit, and physionet. *Circulation*, 101(23):e215–e220, 2000.

[15] R. C. Gonzalez, R. E. Woods, and S. L. Eddins. Image databases. *at available: http://www. imageprocessingplace. com*, 2010.

[16] A. Grossmann and J. Morlet. Decomposition of hardy functions into square integrable wavelets of constant shape. *SIAM journal on mathematical analysis*, 15(4):723–736, 1984.

[17] N. E. Huang and Z. Wu. A review on hilbert-huang transform: Method and its applications to geophysical studies. *Reviews of geophysics*, 46(2), 2008.

[18] N. E. Huang, S. Zheng, S. R. Long, M. C. Wu, H. H. Shih, Q. Zheng, N. C. Yen, C. C. Tung, and H. H. Liu. The empirical mode decomposition and the hilbert spectrum for nonlinear and non-stationary time series analysis. In *Proceedings of the Royal Society of London A: mathematical, physical and engineering sciences*, volume 454, pages 903–995. The Royal Society, 1998.

[19] Y. Lei, J. Lin, Z. He, and M. J. Zuo. A review on empirical mode decomposition in fault diagnosis of rotating machinery. *Mechanical Systems and Signal Processing*, 35(1):108–126, 2013.

[20] D. C. Lin, Z. L. Guo, F. P. Ang, and F. L. Zeng. Elimination of end effects in empirical mode decomposition by mirror image coupled with support vector regression. *Mechanical Systems and Signal Processing*, 31:13–28, 2012.

[21] D. P. Mandic, N. ur Rehman, Z. Wu, and N. E. Huang. Empirical mode decomposition-based time-frequency analysis of multivariate signals: The power of adaptive data analysis. *IEEE signal processing magazine*, 30(6):74–86, 2013.

[22] M. K. Molla and K. Hirose. Single-mixture audio source separation by subspace decomposition of hilbert spectrum. *IEEE Transactions on Audio, Speech, and Language Processing*, 15(3):893–900, 2007.

[23] G. Rilling and P. Flandrin. On the influence of sampling on the empirical mode decomposition. In *Acoustics, Speech and Signal Processing, 2006. ICASSP 2006 Proceedings. 2006 IEEE International Conference on*, volume 3, pages III–III. IEEE, 2006.

[24] G. Rilling and P. Flandrin. Emd toolbox. 2007. [Online; accessed 2007].

[25] G. Rilling and P. Flandrin. One or two frequencies? the empirical mode decomposition answers. *IEEE transactions on signal processing*, 56(1):85–95, 2008.

[26] G. Rilling, P. Flandrin, and P. Goncalves. On empirical mode decomposition and its algorithms. In *IEEE-EURASIP workshop on nonlinear signal and image processing*, volume 3, pages 8–11. IEEER, Grado, Italy, 2003.

[27] J. G. Robson. Spatial and temporal contrast-sensitivity functions of the visual system. *Josa*, 56(8):1141–1142, 1966.

[28] C. M. Sweeney-Reed and S. J. Nasuto. A novel approach to the detection of synchronisation in eeg based on empirical mode decomposition. *Journal of computational neuroscience*, 23(1):79–111, 2007.

[29] E. C. Titchmarsh et al. *Introduction to the theory of Fourier integrals*, volume 2. Clarendon Press Oxford, 1948.

[30] K. Vasudevan and F. A. Cook. Empirical mode skeletonization of deep crustal seismic data: Theory and applications. *Journal of Geophysical Research: Solid Earth*, 105(B4):7845–7856, 2000.

[31] S. Wang, N. Zhang, L. Wu, and Y. Wang. Wind speed forecasting based on the hybrid ensemble empirical mode decomposition and ga-bp neural network method. *Renewable Energy*, 94:629–636, 2016.

[32] Z. Wu and N. E. Huang. Ensemble empirical mode decomposition: a noise-assisted data analysis method. *Advances in adaptive data analysis*, 1(01):1–41, 2009.

[33] R. R. Zhang. Characterizing and quantifying earthquake-induced site nonlinearity. *Soil Dynamics and Earthquake Engineering*, 26(8):799–812, 2006.